Regulation of potassium homeostasis in *Caulobacter crescentus*

Alex Quintero-Yanes[1+], Madeline Collignon[1], Loïc Léger[1], Aurélie Mayard[1], Régis Hallez[1,2,$,#]

[1]Bacterial Cell cycle & Development (BCcD), Biology of Microorganisms Research Unit (URBM), Namur Research Institute for Life Science (NARILIS), University of Namur, Namur (5000), Belgium.

[2]WELBIO, University of Namur, Namur (5000), Belgium

[+] *ORCID ID: 0000-0002-8350-0881*

[$] *ORCID ID: 0000-0003-1175-8565*

[#]Corresponding author: Tel: +32 81 724 244; E-mail: regis.hallez@unamur.be

Short title: Potassium homeostasis in *C. crescentus*.

Key words: Potassium transport, two-component system, Kup, KdpE, KdpD

Abstract

Potassium (K^+) is an essential physiological element determining membrane potential, intracellular pH, osmotic/turgor pressure, and protein synthesis in cells. Nevertheless, K^+ homeostasis remains poorly studied in bacteria. Here we describe the regulation of potassium uptake systems in the oligotrophic α-proteobacterium *Caulobacter crescentus* known as a model for asymmetric cell division. We show that *C. crescentus* can grow in concentrations from the micromolar to the millimolar range by essentially using two K^+ transporters to maintain potassium homeostasis, the low affinity Kup and the high affinity Kdp uptake systems. When K^+ is not limiting, we found that the *kup* gene is essential while *kdp* inactivation does not impact the growth. In contrast, *kdp* becomes critical but not essential and *kup* dispensable for growth in K^+-limited environments. However, in the absence of *kdp*, mutations in *kup* were selected to improve growth in K^+-depleted conditions, likely by improving the affinity of Kup for K^+. In addition, mutations in the KdpDE two-component system, which regulates *kdpABC* expression, suggest that the inner membrane sensor regulatory component KdpD works as a kinase in early stages of growth and as a phosphatase to regulate transition into stationary phase. Our data also show that KdpE is not only phosphorylated by KdpD but also by another non-cognate histidine kinase. On top of this, we determined the KdpE-dependent and independent K^+ transcriptome as well as the direct targets of KdpE. Together, our work illustrates how an oligotrophic bacterium responds to fluctuation in K^+ availability.

39 ## Introduction

40 Potassium (K^+) is the most abundant monovalent cation within living cells (Danchin &
41 Nikel, 2019, Epstein, 2003) and it is essential to set the membrane potential and
42 intracellular pH (Bakker & Mangerich, 1981, Booth, 1999, Epstein, 2003, Ochrombel
43 *et al.*, 2011). As K^+ also emerges as an important regulator of bacterial physiology in
44 view of its role in diverse processes (Castaneda-Garcia *et al.*, 2011, Dominguez-
45 Ferreras *et al.*, 2009, Feng *et al.*, 2022, Gries *et al.*, 2013, Humphries *et al.*, 2017, Liu
46 *et al.*, 2013, MacGilvary *et al.*, 2019, Prindle *et al.*, 2015, Quintero-Yanes *et al.*, 2019,
47 Rasmussen, 2023, Su *et al.*, 2009, Valente & Xavier, 2016) including biofilm formation,
48 chemotaxis, cell to cell communication or virulence, it is therefore expected that K^+
49 transport is tightly regulated.

50 In bacteria, the KdpDE two-component system (TCS) responds to potassium depletion
51 by regulating the expression of the cognate high-affinity K^+ transporter KdpFABC
52 (Pedersen *et al.*, 2019). This inner membrane complex consists of four subunits all
53 encoded in the same operon, often together with the *kdpDE* genes (Ali *et al.*, 2017,
54 Dani *et al.*, 2017). In *Escherichia coli*, KdpD was shown to act as a dual sensor for K^+,
55 which independently regulates both enzymatic activities. Whereas the kinase activity
56 was inhibited by extracellular K^+, phosphatase activity was stimulated by intracellular
57 K^+ (Schramke *et al.*, 2016). This ultimately determines the phosphorylation status of
58 the response regulator KdpE and thus provides a tight regulation of *kdpFABC*
59 expression and as well as a robust homeostasis in fluctuating environments (Schramke
60 *et al.*, 2016).

61 Other K^+ transporters have been described in detail in Gram-negative bacteria, such
62 as the inner membrane low-affinity Trk and Kup systems for uptake, and the KefB efflux

63 pump. The Trk potassium uptake system is highly conserved in bacteria and works in
64 a multi-subunit complex comprising the TrkG/H, TrkA and TrkE proteins. TrkH (an extra
65 copy known as TrkG is found in *E. coli*) is the trans-membrane transporter unit, which
66 interacts with the NAD^+- and NADH-binding peripheral protein TrkA and the ATP-
67 binding protein TrkE in the cytoplasmic leaflet to control extracellular potassium uptake
68 when high extracellular concentrations of K^+ are available (Bossemeyer *et al.*, 1989a,
69 Dosch *et al.*, 1991, Harms *et al.*, 2001). On the other hand, Kup is a single protein,
70 constitutively expressed and thought to function as K^+/Na^+ symporter (Dosch *et al.*,
71 1991, Schleyer & Bakker, 1993, Zakharyan & Trchounian, 2001).
72 Recently, it was reported that glutathione controls cell division via negative regulation
73 of KefB in the Gram-negative oligotrophic α-proteobacterium *Caulobacter crescentus*
74 (3). Indeed, mutants unable to synthesize glutathione led to cell filamentation and
75 decreased intracellular K^+ levels. Interestingly, these phenotypes were suppressed by
76 mutations in the KefB efflux pump, suggesting that K^+ homeostasis is crucial for
77 bacterial cell cycle regulation. *C. crescentus* has been extensively used as a model for
78 cell cycle studies since it divides asymmetrically to give birth to a larger sessile stalked
79 cell and a smaller flagellated swarmer cell (1). DNA replication and cell division take
80 place only in sessile stalked cells whereas the swarmer cells remain in a non-
81 replicative but chemotactically active and motile phase able to explore new
82 environments. Once swarmer cells find a suitable – resourceful – habitat for
83 reproduction, they differentiate into stalked cells and concomitantly start DNA
84 replication. In contrast, upon deprivation of environmental resources, the swarmer cells
85 do not differentiate into replicative stalked cells.

86 In this study, we characterized the response of *Caulobacter* cells grown in
87 environments containing what we defined as limiting, abundant and excessive K^+
88 concentrations. *In silico* analyses revealed that *C. crescentus* does not have Trk
89 system components but encodes a putative transporter with a cytoplasmic TrkA-like
90 domain. Moreover, in addition to the KefB and KefC efflux pumps, we found genes
91 predicted to code for a Kup and a KdpABC transporters as well as a KdpDE TCS. We
92 generated mutants of these predicted K^+ transporters and assessed their fitness in
93 limiting and abundant K^+ environments. We also characterized the KdpDE system and
94 determined its regulon by ChIP-seq and RNA-seq.

95

96 ## Results

97 **Growth of *C. crescentus* at different K^+ concentrations**

98 To primarily assess the impact of K^+ on *C. crescentus* fitness, the wild-type (WT) strain
99 was grown in K^+-free minimal media (M2G-K) supplemented with K^+ at different
100 concentrations using either KCl or a combination of K_2HPO_4 and KH_2PO_4 (K_2HPO_4 +
101 KH_2PO_4) like the one used in standard M2G minimal media (**Fig. 1**). First, when
102 phosphate salts were used as K^+ source, we observed that compared to M2G, which
103 contains 7 mM K^+, growth started to be significantly impaired at K^+ concentrations
104 below or equal to 0.025 mM and above or equal to 7 mM (**Fig. 1AB**). Second, by using
105 KCl, we found different K^+ concentrations critical for growth since the WT already failed
106 to grow at 0.1 mM but supports growth up to 25 mM (**Fig. 1CD** and **Fig. S1A**).
107 Notwithstanding these differences likely due to the $PO4^{3-}$ and Cl^- counter-anions, the
108 growth of the WT at K^+ concentrations ranging from 0.5 mM to 5 mM was
109 indistinguishable from the one in M2G, that is 7 mM (**Fig. 1**). Therefore, based on these

110 data, we will use in this study potassium phosphate salts at 0.025 mM and 0.5 mM
111 respectively as limiting and abundant concentrations while KCl will be used at 50 mM
112 as excessive concentration.
113
114 **K^+ transport and regulation systems in *C. crescentus***
115 By using *in silico* analyses, we found in the genome of *C. crescentus* NA1000
116 (NC_011916.1) several genes encoding potential K^+ uptake (*kup* and *kdpABCDE*) or
117 efflux (*kefB*, *kefC* and *kefG*) systems (**Fig. 2**). Although Trk orthologs were not found,
118 a putative transporter (CCNA_01688) containing a cytoplasmic TrkA-like domain was
119 identified (**Fig. 2**). Based on the function of the Kdp, Kef, Kup and Trk systems in other
120 bacteria (Bossemeyer *et al.*, 1989b, Cao *et al.*, 2011, Epstein, 2003, MacGilvary *et al.*,
121 2019, Roosild *et al.*, 2010), we predicted that transport of K^+ in *C. crescentus* occurs
122 via CCNA_01688, KefBG, KefC and Kup when potassium is abundant in the
123 environment (**Fig. 2A**) whereas the Kdp system might be inactive (**Fig. 2B**) (Heermann
124 & Jung, 2010, Roe *et al.*, 2000). In contrast, K^+-depleted conditions should activate the
125 KdpDE TCS and trigger expression of the high affinity KdpABC transporter (**Fig. 2C)**
126 (Laimins *et al.*, 1981).
127 To test these predictions, we first constructed knock-out (KO) mutants for all the K^+
128 transport and regulatory systems described above. We successfully inactivated all
129 these genes except *kup*, suggesting it might be essential at least at the K^+
130 concentration found in the complex media PYE used to construct the KO strains. Note
131 that a Δ*kefB* and Δ*kdpABCDE* (hereafter referred to as Δ*kdp*) were respectively used
132 as KefBG and Kdp inactive mutants (**Fig. 2C**). Then, we measured the growth for the
133 mutants in M2G-K supplemented with limiting (0.025 mM), abundant (0.5 mM) or

134 excessive (50 mM) K^+ concentrations (**Fig. 3**). In limiting K^+ conditions, only Δ*kdp* had
135 a strong growth delay (**Fig. 3A**) whereas all the KO mutants grew as good as the WT,
136 both in minimal and complex media supplemented with abundant K^+ concentrations
137 (**Fig. 3B** and **Fig. S1B**). However, and as far as we know in contrast to what is
138 described in other bacteria, a *kdp* inactive mutant could still grow in such limiting
139 conditions, suggesting that another transporter is used in K^+-depletion conditions. At
140 excessive K^+ concentration, we found that (i) Δ*CCNA_01688* had a slight growth delay;
141 (ii) Δ*kdp* had a lower plateau and (iii) Δ*kefC* barely grew in comparison to WT (**Fig.**
142 **3C**). Interestingly, the growth delay of Δ*CCNA_01688* and the lower plateau of Δ*kdp*
143 were not observed in complex PYE media supplemented with an excess of K^+ whereas
144 Δ*kefC*, like in minimal medium, did not grow (**Fig. S1C**).
145

146 **K^+-dependent essential genome**

147 Transposon mutagenesis coupled to next-generation sequencing (Tn-seq) were used
148 to determine a core set of genes important for adaptation and response to abundant
149 or limiting K^+ condition. Isolated colonies harbouring transposon insertions were grown
150 on and collected from solid agar plates. We used M2G-K with 1 % agar concentration
151 to lower as much as possible K^+ traces from the agar in our experiment. Indeed, even
152 at 1% agar, the K^+ traces were sufficient to allow WT cells to grow without exogenous
153 source of K^+ (on M2G-K, **Fig. 4A**). In contrast, at least 0.025 mM K^+ had to be
154 supplemented to M2G-K to allow growth of Δ*kdp* while at 0.5 mM K^+, both the mutant
155 and the WT grew similarly to the growth observed on regular M2G which contains 7
156 mM K^+ (**Fig. 4A**). Therefore, we decided to use M2G-K without exogenous K^+ and M2G
157 plates respectively as the limiting and abundant K^+ conditions for the Tn-seq (**Fig. 4A**).

158 We did calculations on the ratio of transposon (Tn) insertions per base pair (# Tn
159 insertions / bp) for internal 80% of each ORF in each condition (M2G and M2G-K)
160 (**Table S1**). As in studies performed in other bacteria, we analysed the frequency of Tn
161 insertions and observed a bimodal distribution that allowed us visualizing two clusters
162 of genes in each condition, one with low density of Tn insertions (considered as
163 essential genes) and the other one with a higher density (considered as non-essential
164 genes) (**Figure S2A)**. Based on this frequency of Tn insertions, we used Ward's
165 clustering analysis (Curtis & Brun, 2014) and defined three fitness cost categories, that
166 is (i) essential, (ii) high fitness cost (HFC) and (iii) non-essential. For the M2G library,
167 genes with values of Tn insertions / bp ≤ 0.01333333 were considered as essential,
168 0.01333779 ≤ and ≤ 0.04063018 as HFC, and ≥ 0.04081632 as non-essential. For the
169 M2G-K library, genes values of ≤ 0.0047112 were considered as essential, 0.0047909
170 ≤ and ≤ 0.0211178 as HFC, and ≥ 0.0215792 as non-essential (**Figure 4B** and **Table**
171 **S1**). Among the 4186 annotated genes in *C. crescentus*, the percentage of essential
172 genes in both media (M2G and M2G-K) was similar (~12 %), whilst the percentage of
173 HFC genes was lower (~7 %) in M2G-K than in M2G (~13 %). Hence, the percentage
174 of non-essential genes was higher in M2G-K (~ 81 %) than in M2G-K (~75 %). The
175 shift from the HFC to the non-essential category in *C. crescentus* cells grown in M2G-
176 K could be explained by the reduction of osmotic stress in this medium. Indeed, we
177 showed recently that M2G generates a cell envelope stress for *C. crescentus* due to
178 the high content of monovalent cations (Quintero-Yanes *et al.*, 2022).

179 Genes with known or predicted biological functions were grouped according to the
180 classification of cluster of orthologues groups (COG) (**Fig S2B**). This allowed to
181 highlight biological functions that are enriched in abundant and limited K^+ conditions.

182 Overall, the COG enrichment in the three fitness categories (Essential– E, High Fitness
183 Cost– HFC and Non-Essential– N-E) was essentially similar in both M2G and M2G-K
184 media. The C group "energy production and conversion" genes was the most abundant
185 for all the fitness categories in M2G-K, as well as for E and N-E genes in M2G, while
186 for HFC it was the second most abundant, after the J group "translation, ribosomal
187 structure and biogenesis".

188 By comparing the gene pool in each category for each media, we identified a set of
189 537 genes that changed their fitness cost from M2G to M2G-K and vice versa (**Fig. 4C**
190 and **Table S2**), including 153 genes which became exclusively essential (28.5 %), 153
191 HFC (28.5 %) and 231 non-essential (43 %) in M2G-K. First, we observed that the TCS
192 genes *chvGI*, known to be HFC in M2G due to its response to hyperosmotic stress
193 (Quintero-Yanes *et al.*, 2022), became N-E in M2G-K, thereby supporting that M2G-K
194 is a hypo-osmotic environment compared to M2G. Second, all the *kdp* genes
195 categorised as N-E genes in M2G became essential in M2G-K except *kdpD* which
196 became HFC. In contrast, *kup* moved from the HFC category in M2G to N-E one in
197 M2G-K. This confirms the importance of the Kdp and Kup systems repectively in
198 limiting and abundant K^+ conditions. Considering the conservation of the *kdp* system
199 in bacteria, it is intriguing that *kdpD* – encoding the HK component – did not have the
200 same fitness cost in M2G-K than the genes coding for the transporter (*kdpABC*) and
201 the response regulator (*kdpE*) components. While this supports that KdpE likely
202 regulates, directly, the expression of *kdpABC* genes, it suggests that KdpD and KdpE
203 have different regulatory effects on growth in K^+-depleted environments. Finally, we
204 did not observed changes in fitness for the other predicted potassium transport
205 systems since all of them were categorised as N-E genes in both M2G and M2G-K,

206 further supporting that CCNA_01688, KefBG and KefC are not important for growth in
207 abundant and limiting K^+ conditions.

208

209 **Kup becomes dispensable in limiting K^+ conditions**

210 Tn-seq data suggest that inactivation of *kup* gene could be facilitated at limiting K^+
211 concentrations (**Fig. 4B**, **Tables S1** and **S2**). Kup has been described in different
212 bacteria as the major K^+ transporter, essential in hyperosmotic conditions using
213 sucrose as osmotic stressor (de Oliveira *et al.*, 2017, Trchounian & Kobayashi, 1999).
214 Moreover, in a previous study, we found that the TCS ChvGI in *C. crescentus* positively
215 controls the expression of *kup* in hyperosmotic conditions (Quintero-Yanes *et al.*,
216 2022). In agreement with this, we could not obtain a Δ*kup* strain by using a markerless,
217 SacB-dependent recombination approach on complex media (PYE) plates
218 supplemented with 3% sucrose for the counterselection. Since addition of sucrose
219 considerably increases the osmolality of the media (Hocking *et al.*, 2012), we aimed to
220 construct a Δ*kup* mutant by lowering osmolytes in the media, that is on M2G-Na-K
221 (lacking both Na_2HPO_4 and KH_2PO_4) plates supplemented with 0.5 % sucrose. In these
222 conditions, we successfully generated Δ*kup* mutant candidates that were then tested
223 for growth at different K^+ regimes. Interestingly, we observed that the Δ*kup* mutant
224 grew in limiting K^+ concentration (M2G-K supplemented with 0.025 mM K^+), although
225 at a slower growth rate but with a higher plateau compared to the WT (**Fig. 5A**). As
226 expected from the Tn-seq data, we found that Δ*kup* failed to grow when exposed to
227 abundant and excessive K^+ concentrations (**Fig. 5A**). We also confirmed that Kup is
228 essential in hypertonic conditions since the mutant did not grow in limiting K^+ conditions

229 when 3% sucrose were added. (**Fig. 5A**). Furthermore, we also observed that
230 overexpression of *kup* in WT is detrimental for growth in limiting K^+ conditions (**Fig.**
231 **5B**). Altogether, these data indicate that Kup allows potassium uptake in abundant and
232 excessive K^+ conditions but can be detrimental for unknown reasons at limiting K^+
233 concentrations.
234 While characterizing the growth of Δ*kdp* cells on M2G-K plates (**Fig. 4A**), we
235 inadvertently selected growth suppressors. These suppressors improved the growth of
236 Δ*kdp* in limiting K^+ conditions (**Fig. 5C**). Whole genome sequencing analyses of several
237 of these suppressors allowed the identification of three mutations in *kup*: kup_{A87P},
238 kup_{G253S} and kup_{S456R}. Altogether, these data indicate that Kup allows potassium
239 uptake in abundant and excessive K^+ conditions but unexpectedly also works at low –
240 limiting – K^+ concentrations, and that single point mutations in Kup likely improve its
241 affinity for K^+.
242
243 **K^+- and KdpE-dependent regulons**
244 To further characterise the response of *C. crescentus* to K^+-depleted conditions, we
245 performed RNA-seq on RNA samples extracted from cells grown in minimal media in
246 K^+ limiting or abundant conditions. In our experiment, we identified a total of 594 genes
247 – 385 upregulated and 209 downregulated – whose expression was impacted upon K^+
248 limitation with at least a 2-fold change (FC ≥ 2) and a false-discovery rate (FDR) lower
249 than 5% ($P_{adj} \leq 0.05$) (**Fig. 6A**). As expected, this experiment confirmed that the
250 expression of *kdp* genes was strongly induced in the K^+-depleted medium. Among the
251 other upregulated genes, we found genes coding for the phosphate starvation protein
252 PhoH (CCNA_02727), a xylose isomerase family protein (CCNA_01701), a TonB-

253 dependent receptor (TBDR, CCNA_01859), an AraC family transcription regulator
254 (CCNA_01858) and hypothetical proteins (CCNA_03313 and CCNA_03970) (**Fig. 6A**
255 and **Table S3A**). Among the top downregulated candidates, we found genes
256 expressing a small RNA (CCNA_R0158), a hemin receptor (CCNA_02277), a putative
257 transporter (CCNA_03022), a protein with a calcium binding EF Hand binding domain
258 (CCNA_02274) and the chaperons GroES (CCNA_00722) and GroEL (CCNA_00721)
259 (**Fig. 6A** and **Table S3B**).

260 As our results suggest that the Kdp system is important for growth upon K^+ depletion,
261 we also performed RNA-seq experiments with a Δ*kdpE* mutant grown in M2G-K
262 supplemented with limiting K^+ concentrations. Then, we compared the RNA enrichment
263 in Δ*kdpE vs* WT to determine which genes are affected by KdpE in a K^+-depleted
264 condition using FC ≥ 1.5 and $P_{adj} \leq 0.05$ as parameters. Compared to WT, we found
265 83 upregulated and 50 downregulated genes in Δ*kdpE* grown in the K^+-depleted media
266 (**Fig. 6B** and **Tables S4AB**). Among the 50 downregulated genes in Δ*kdpE* (**Table**
267 **S4B**), 72% (36/50) were also found in the regulon of the WT starved for K^+, 19
268 upregulated (including *kdp* genes; **Table S3A**) and 17 downregulated (**Table S3B**).
269 This suggests that KdpE is strictly required to activate the expression of the 19 genes
270 in a K^+-depleted environment. On the contrary, the 17 other genes that are repressed
271 in WT cells upon K^+ depletion are even further downregulated in the absence of KdpE,
272 suggesting that KdpE limits the repression of these genes. The expression of the last
273 14 genes was insensitive to K^+ concentration while downregulated in Δ*kdpE* (**Tables**
274 **S4AB**), suggesting that they are positively regulated by KdpE but independently of the
275 K^+ concentration. Among the 83 upregulated genes in Δ*kdpE* (**Table S4A**), only ~36%
276 (30/83) were also found in the regulon of the WT starved for K^+, 12 downregulated

277 (including *groEL* and *groES* genes; **Table S3B**) and 18 upregulated (**Table S3A**). This
278 indicates KdpE is required to repress the first 12 genes upon K^+ depletion while it limits
279 the activation of the other 18 genes in a K^+-depleted environment. The remaining 53
280 upregulated genes in Δ*kdpE* (**Tables S4AB**) were insensitive to K^+ availability,
281 suggesting that they are likely repressed by KdpE but independently of the K^+
282 concentration.
283 Surprisingly, the vast majority (528 genes; 88.9 %) of the 594 genes whose expression
284 changed in the WT grown in K^+ limiting conditions seems to be KdpE-independent,
285 suggesting that other regulators, yet to be discovered, are activated upon K^+ depletion.
286 An alternative explanation might be that Δ*kdpE* cells exposed to limiting K^+
287 concentration suffer from a general stress response, which ultimately leads to global
288 transcriptional changes. This could also explain why half of the 163 genes (67/133)
289 found in the Δ*kdpE* regulon were not identified in the WT regulon.
290 In order to unveil genes whose expression is directly regulated by KdpE, we identified
291 the DNA regions bound by KdpE using ChIP-seq. For that, we first constructed strains
292 in which *kdpE* was expressed under the xylose inducible promoter (P_{xylX}::*kdpE*) in a
293 Δ*kdpE* Δ*xylX* background. Inactivating *xylX* avoids xylose consumption by *C.*
294 *crescentus* as a carbon source thereby allowing constant expression of *kdpE* upon
295 induction. Expression of *kdpE* from P_{xylX} efficiently complemented the growth of both
296 strains in the presence of xylose since Δ*kdpE* Δ*xylX* P_{xylX}::*kdpE* cells grew similarly to
297 the WT or Δ*xylX* cells whereas Δ*kdpDE* Δ*xylX* P_{xylX}::*kdpE* cells grew at a higher plateau
298 (**Fig. S3A**) like Δ*kdpD* cells (see below). Moreover, using polyclonal anti-KdpE
299 antibodies, KdpE was easily detected by western blot in both strains although KdpE
300 protein levels were lower in Δ*kdpDE* Δ*xylX* than in Δ*kdpE* Δ*xylX* (**Fig. S3B**), suggesting

301 that KdpD has a global positive impact on KdpE levels. It is noteworthy that KdpE was
302 undetectable in WT strain, indicating that P_{xylX}::*kdpE* leads to KdpE overexpression
303 upon xylose induction.
304 A total of 110 and 146 DNA binding sites were respectively detected in the Δ*kdpE*
305 Δ*xylX* P_{xylX}::*kdpE* and Δ*kdpDE* Δ*xylX* P_{xylX}::*kdpE* strains grown in K^+ limiting conditions
306 (**Fig. 6C**; **Tables S5** and **S6**). About a third of the DNA regions bound by KdpE
307 identified in both strains – 40 out of 110 (36.4%) found in Δ*kdpE* Δ*xylX* P_{xylX}::*kdpE* and
308 46 out of 146 (31.5%) found Δ*kdpDE* Δ*xylX* P_{xylX}::*kdpE* – are located in the close vicinity
309 of genes whose expression showed a FC ≥ 1.5 in RNA-seq experiments (highlighted
310 in green in **Tables S5** and **S6**), supporting that these regions are indeed KdpE-binding
311 sites.
312 The highest numbers of reads were found in the *kdp* promoter region, not only in Δ*kdpE*
313 Δ*xylX* P_{xylX}::*kdpE* cells but more surprisingly also in Δ*kdpDE* Δ*xylX* P_{xylX}::*kdpE* cells.
314 Even more surprising is the fact that the peak for Δ*kdpDE* Δ*xylX* P_{xylX}::*kdpE* was higher
315 than in Δ*kdpE* Δ*xylX* P_{xyl}::*kdpE* (**Fig. 6C**). In fact, this is true for most of if not all the
316 regulated genes, but the difference was particularly important for the *kdp* promoter
317 (**Fig. 6D**), suggesting that KdpE could be hyperphosphorylated in the absence of KdpD
318 and therefore that KdpD mainly acts as a negative regulator of KdpE~P. Moreover, it
319 indicates that, although P_{kdp} is the main target of KdpE, multiple other genes are
320 potential direct targets of KdpE. Analysis of the top 50 sequences identified in the ChIP-
321 seq with the Δ*kdpE* Δ*xylX* P_{xylX}::*kdpE* strain using MEME allowed the identification of
322 the conserved DNA motif TCGAMRACGCSMKC likely bound by KdpE (**Fig. 6E**). For
323 the peak in the vicinity of the *kdpABCDE* operon (top hit of the analysis), the KdpE

324 motif was located 113 bp upstream of the *kdpA* start codon, within the gene
325 CCNA_01662 (**Fig. 6E**).
326
327 ***C. crescentus* KdpD regulates KdpE both positively and negatively**
328 To further assess the role of the *C. crescentus* Kdp system in K^+-limiting conditions,
329 we first constructed KO mutants of the transport complex (Δ*kdpABC*) and the TCS
330 (Δ*kdpDE*) genes. In comparison to the WT, both Δ*kdpABC* and Δ*kdpDE* mutants had
331 a growth delay at limiting but not at abundant K^+ concentration (**Fig. 7A** and **Fig. S4A**).
332 Moreover, both mutants grew similarly, suggesting that the *kdpABC* is not expressed
333 in the absence of the TCS, as described in other bacteria.
334 To study the HK *kdpD* and RR *kdpE* genes independently of each other, we
335 constructed single KO mutants, Δ*kdpD* and Δ*kdpE*. Deletion of *kdpE* resulted in a
336 similar growth delay than the ones displayed by Δ*kdpABC*, Δ*kdpDE* and Δ*kdpABCDE*
337 (**Fig. 7A** and **Fig. S4B**). On the contrary, Δ*kdpD* behave differently since compared to
338 WT, it had a slight but reproducible growth delay in exponential phase while it later
339 reached a higher plateau in stationary phase (**Fig. 7A**). This peculiar growth behaviour
340 was complemented by expressing *kdpD* from the native *kdp* promoter (P_{kdp}::*kdpD*) on
341 a replicative and low-copy number plasmid in a Δ*kdpD* background (**Fig. 7B**).
342 Complementation of the Δ*kdpE* mutant was achieved by expressing *kdpE* from the
343 xylose inducible promoter (P_{xylX}::*kdpE*) either in a Δ*kdpE* or a Δ*kdpDE* background.
344 While the growth defect of Δ*kdpE* was fully complemented, even in the absence of the
345 xylose inducer, expressing back *kdpE* in Δ*kdpDE* cells led to the same growth
346 behaviour than the single Δ*kdpD* mutant, that is a slight growth delay in exponential
347 phase and a higher plateau in stationary phase (**Fig. 7C** and **Fig. S4C**). In addition,

348 the fact that Δ*kdpE* is epistatic on Δ*kdpD*, since Δ*kdpDE* grew as poor as Δ*kdpE* or
349 Δ*kdpABC* (**Fig. 7A**), shows KdpE is entirely responsible for the Δ*kdpD* phenotypes.
350 Together, these data support that both components of the TCS are important for WT
351 growth in K^+-depleted environments and suggest that KdpD and KdpE have
352 antagonistic roles for growth in such conditions. Kdp regulatory proteins KdpD and
353 KdpE were further analysed by identifying domains and their organisation. Comparison
354 of Pfam features highlighted that the KdpD sequence of *C. crescentus* lacks the
355 cytoplasmic GAF domain known to be linked to the DHp domain in *E. coli* [103]. Also,
356 multiple sequence alignments enabled to locate the conserved catalytic –
357 phosphorylatable – residues in both the HK (KdpD) and the RR (KdpE), that is
358 respectively the histidine 670 (His670) and the aspartate 56 (Asp56). To better
359 understand the KdpDE regulatory mechanism, we constructed *kdpD and kdpE*
360 catalytic point mutants and assessed their impact on growth in abundant and limiting
361 K^+ conditions. In agreement with what we observed with the KO mutants, all the
362 catalytic mutants grew as good as the WT in abundant K^+ conditions (**Fig. S4D**). At
363 limiting K^+ concentrations however, the phospho-ablative mutant of KdpE ($kdpE_{D56A}$)
364 had a strong growth delay, similar to the one displayed by Δ*kdpE* (**Fig. 7D** and **Fig.**
365 **S4E**). In contrast, the phospho-mimetic mutant ($kdpE_{D56E}$) grew similarly to the WT up
366 to the late exponential phase, to finally reach a higher final OD comparable to the one
367 observed with Δ*kdpD* grown in same conditions (**Fig. 7D** and **Fig. S4E**). As expected,
368 a KdpD catalytically dead mutant ($kdpD_{H670N}$) phenocopied Δ*kdpD* in limited K^+ (**Fig.**
369 **7D** and **Fig. S4E**). Since $kdpE_{D56A}$ cells had a much stronger growth delay than Δ*kdpD*
370 or $kdpD_{H670N}$, it indicates that KdpE is still phosphorylated despite the absence of KdpD
371 kinase activity. Thus, KdpE is very likely phosphorylated by another – non-cognate –

372 HK. On the other hand, the fact that *kdpE*$_{D56E}$ cells grew slightly but reproducibly better
373 than Δ*kdpD* and *kdpD*$_{H670N}$ suggests that KdpD also phosphorylates KdpE, at least
374 during the early exponential phase of growth. Thus, KdpD might (i) phosphorylate
375 KdpE in early exponential phase, with at least another HK, and (ii) mainly act as a
376 phosphatase on KdpE~P in late exponential phase, likely to downregulate the
377 expression of *kdp* and restrict growth in K^+-limiting conditions.

378 To test this hypothesis, we constructed a KdpD kinase-deficient but phosphatase
379 active mutant (K^-/P^+) by replacing a conserved phenylalanine residue by a leucine
380 residue (*kdpD*$_{F832L}$) in a way reminiscent to what was described for another HK
381 encoding gene, *pleC*$_{F778L}$ (Matroule *et al.*, 2004). Interestingly, we found that unlike the
382 *kdpD*$_{H670N}$, *kdpD*$_{F832L}$ cells failed to reach a higher plateau in stationary phase (**Fig. 7D**
383 and **Fig. S4E**), strongly supporting our hypothesis that KdpD primarily works as a
384 phosphatase in late exponential phase. Moreover, the K^-/P^+ mutant *kdpD*$_{F832L}$ grew
385 better than *kdpE*$_{D56A}$ and Δ*kdpE* mutants in low K^+ conditions (**Fig. 7D** and **Fig. S4E**),
386 supporting that there is indeed at least another HK that phosphorylates KdpE. Finally,
387 the fact that the *kdpD*$_{F832L}$ mutant had a growth delay compared to WT suggests that
388 KdpD also acts as a kinase for KdpE in early exponential phase (**Fig. 7D** and **Fig.**
389 **S4E**). However, we cannot rule out the possibility that the phosphatase activity of
390 KdpD$_{F832L}$ is impacted by the mutation. For instance, it might be stronger than the WT
391 thereby interfering with the phosphorylation levels of KdpE in early exponential phase.
392 Nevertheless, our results altogether indicate that (i) KdpD works both as a kinase and
393 phosphatase to control KdpE phosphorylation (KdpE~P) levels depending on the
394 growth phase and K^+ availability and that (ii) KdpE can be phosphorylated by (an)other
395 non-cognate HK(s) for regulating K^+ transport in K^+-depleted environments.

396

397 **KdpD-dependent activation of the *kdp* promoter in low K^+ conditions**

398 In order to study the Kdp system at the transcriptional level, a plasmid carrying a
399 P_{kdp}::*lacZ* reporter fusion was introduced in the different mutant strains, cells were
400 grown in limiting and abundant K^+ concentrations and β-galactosidase activity was
401 measured. Consistent with the idea that the Kdp system is a high-affinity potassium
402 transporter, P_{kdp} basal activity in WT cells was barely detectable (~300 Miller Units) at
403 abundant K^+ concentration while it was strongly induced in WT (~9.000 Miller Units) or
404 in Δ*kdpABC* cells (~10.500 Miller Units) upon K^+ depletion (**Fig. 8A**). In contrast, P_{kdp}
405 activity was completely annihilated in Δ*kdpE* and $kdpE_{D56A}$ cells (**Fig. 8A**), indicating
406 that phosphorylated KdpE (KdpE~P) is strictly required for *kdp* expression both in
407 limiting and abundant K^+ conditions. In support of that, the basal activity of P_{kdp} at
408 abundant K^+ concentration was 10 times higher (~3.000 Miller Units) in $kdpE_{D56E}$ cells
409 than in WT cells (**Fig. 8A**). Interestingly, P_{kdp} was still active at low K^+ concentration in
410 a Δ*kdpD,* $kdpD_{H670N}$, and $kdpD_{F832L}$ background (~4.600, ~4.200, ~4.700 Miller Units,
411 respectively), but not to the same extent than in WT cells (~9.000 Miller Units) (**Fig.
412 8A**). In addition, the basal P_{kdp} activity at abundant K^+ concentration was completely
413 abolished in the strains expressing the K^-/P^+ $kdpD_{F832L}$ variant, suggesting that the
414 KdpD phosphatase activity is counterbalanced by its kinase activity on KdpE in K^+-
415 replenished conditions. In support of that, compared to WT cells grown in abundat K^+
416 condition, the basal P_{kdp} activity was higher when both the hydrolase and kinase
417 activities were inactivated (K^-/P^-), that is in Δ*kdpD* cells and to a lesser extent in
418 $kdpD_{F832L}$ cells.

419 Then, we followed the expression of the P_{kdp}::*lacZ* fusion in WT and *kdp* mutant cells
420 along the growth at limiting K^+ concentration. Despite Δ*kdpABC*, Δ*kdpE* and $kdpE_{D56A}$
421 all poorly grew in limiting K^+ conditions, P_{kdp} was active in Δ*kdpABC* cells to a level
422 comparable to the WT one while P_{kdp} activity was almost undetectable in both *kdpE*
423 mutants (**Fig. 8B**). These data suggest that (i) the Kdp transporter (KdpABC) is not
424 required for *kdp* expression while (ii) the response regulator is, in contrast,
425 indispensable. In support of this, we found the phospho-mimetic mutant of *kdpE*
426 ($kdpE_{D56E}$) displayed a relatively constant but high activity of P_{kdp} alongside the growth
427 curve (**Fig. 8B**).

428 The *kdpD* mutants had a different behaviour. First, compared to WT, the activity of P_{kdp}
429 was Δ*kdpD* cells was lower during early exponential phase but higher in stationary
430 phase (**Fig. 8C**). On the contrary, *kdp* expression was significantly lower both in
431 $kdpD_{H670N}$ (K^-/P^-) and in $kdpD_{F832L}$ (K^-/P^+) during early exponential phase. However,
432 P_{kdp} activity strongly increased only in $kdpD_{F832L}$ cells when reaching the late
433 exponential. Altogether, these results support our hypothesis that (i) KdpD plays dual
434 antagonistic activities on KdpE, as a kinase in early exponential phase and a
435 phosphatase in late exponential phase of growth, and that (ii) KdpE can be
436 phosphorylated by another non-cognate HK all along the growth.

437

438 ## Discussion

439 As the most abundant monovalent cation used by living cells to drive many cellular
440 processes, regulating potassium (K^+) homeostasis is critical for survival. The
441 oligotrophic α-proteobacterium *Caulobacter crescentus*, widely used as a cell cycle

442 model, is cyclically subjected to nutrients deprivation in its natural environments. In
443 contrast to carbon, nitrogen or phosphate, the response of *C. crescentus* to K^+
444 depletion has never been characterised. Here, we first determined the range of K^+
445 concentrations at which *C. crescentus* supports growth. We also identified all the genes
446 predicted to code for proteins involved the transport, the sensing and the regulation of
447 K^+ homeostasis and tested their growth behaviour at low (limiting), optimal (abundant)
448 and high (excessive) K^+ concentrations. Then, we defined the set of genes that (i)
449 become essential and/or (ii) are induced upon K^+-environmental depletion. This
450 allowed us to identify the low affinity and the high affinity K^+ transporters, respectively
451 Kup and KdpABC, as critical components that maintain K^+ homeostasis in *C.*
452 *crescentus*. Finally, we deeply characterized the role played by the two-component
453 (TCS) regulatory system KdpDE in the response to K^+ depletion.

454 By analysing the Tn-Seq data, we found that the COG categories – biological functions
455 – for which the highest number of genes became essential (EG) or high fitness cost
456 (HFCG) upon K^+ limitation (M2G *vs* M2G-K) were (i) C "energy production and
457 conversion" (~1% increase of EG and ~6 % increase of HFCG) and (ii) J "Translation,
458 ribosomal structure and biogenesis" (~2% increase of EG and ~3 % increase of HFCG)
459 (**Table S2**). In fact, it is not so surprising to highlight these two categories as sensitive
460 to K^+ availability. Indeed, ATP concentration and respiration state are two well-known
461 parameters that drive K^+ transport across the membrane. For instance, the electron
462 transport chain determines the membrane potential, which in turn will influence the
463 distribution of other ions across like K^+ that accumulate on the cytoplasmic face of the
464 membrane. This might therefore explain why Tn-insertions in genes coding for subunits
465 of the respiratory chain or the ATP synthase are counter-selected when K^+ become

466 limiting. On top of this, active transport of K^+ across the membrane by the high-affinity
467 transporter consumes a lot of energy provided by ATP, so that decreasing ATP
468 concentration likely has a negative impact on K^+ import. On the other hand, K^+ cations
469 are critical for maintaining the structure and sustaining the function of ribosomes. Not
470 only K^+ is required to stabilize the messenger RNA, the transfer RNAs, the ribosomal
471 RNAs and the ribosomal proteins within the ribosomes, but also to increase
472 proofreading by accommodating the right aminoacyl-tRNA in the ribosomal A-site
473 (Grason *et al.*, 2008, Rozov *et al.*, 2019) . Additionally, many GTPases involved in
474 translation display a K^+-dependent activation of GTP hydrolysis (Danchin & Nikel,
475 2019).Thus, the impact K^+ has on translation could explain the lower Tn insertion
476 density observed in rRNA, tRNA and genes coding for ribosomal proteins in cells grown
477 in limiting on K^+ conditions.

478 Several physiological processes have been described to be K^+-dependent. Besides
479 being required by numerous enzymes related to basic metabolic functions (Danchin &
480 Nikel, 2019, Gohara & Di Cera, 2016), such as for example the pyruvate kinase
481 (Epstein, 2003), K^+ modulates the activity of enzymes involved in bacterial cell cycle.
482 For instance, in *E. coli*, K^+ has been shown to stimulate the polymerisation of the cell
483 division protein FtsZ (Ahijado-Guzman *et al.*, 2013), the activity of the DNA polymerase
484 (Klenow & Henningsen, 1969). Moreover, the DNA supercoiling activity of the DNA
485 gyrase was described to be triggered by K^+ in both *B. subtilis* (Gubaev & Klostermeier,
486 2012) and *Micrococcus luteus* (Liu & Wang, 1978). It was also described as critical for
487 the chaperonin activity of GroEL/GroES (Grason *et al.*, 2008) or DnaK (Feifel *et al.*,
488 1996). Interestingly, we observed that *groEL* and *groES* became essential upon K^+

489 depletion, thereby suggesting that some K^+-dependent mechanisms are conserved in
490 bacteria.

491 KdpDE is the major, if not the only bacterial system described in the literature to
492 respond to limiting K^+ availability. Although KdpE was shown in *E. coli* to regulate
493 expression of the anti-sigma factor Rsd and the ribosome modulation factor Rmf at low
494 K^+ concentrations, thereby allowing KdpE to globally control transcription and
495 translation in limiting K^+, other regulatory systems independent of KdpDE have not
496 been yet described in bacteria. The K^+-dependent regulon of *C. crescentus* allowed us
497 to identify almost 600 genes whose expression changes upon K^+ limitation.
498 Surprisingly, only a small proportion of this regulon depends directly or indirectly on
499 the response regulator KdpE, suggesting that there are unknown transcriptional
500 regulators sensitive to K^+ availability.

501 The analysis of the *C. crescentus* genome allowed us to identify several genes and
502 systems predicted to transport K^+. By systematically characterizing the growth profile
503 of the corresponding mutants in different K^+ regimes, we found that the high affinity
504 Kdp system primarily serves to import K^+ at limiting K^+ concentrations, like in many
505 other bacterial species. Nonetheless, Kdp is unlikely the sole K^+ transport system
506 involved in this context. Despite its growth defect, the Δ*kdpABC* mutant was still able
507 to grow at low K^+ concentration. Since complete depletion of K^+ led to a growth arrest
508 in *C. crescentus*, this implies that K^+ is imported by additional system(s), at least in
509 limiting K^+ conditions. Interestingly, we found that the low affinity Kup transporter
510 became dispensable in such limiting K^+ conditions. However, mutations in Kup have
511 been identified to improve the growth the Δ*kdp* mutant on M2G-K plates (**Fig. 5D**),
512 strongly suggesting that Kup participates to K^+ import when it is poorly available.

513 To test whether Kup is at work at low K^+ conditions, it might be interesting to try to
514 combine Δ*kdp* and Δ*kup* mutations together. Nonetheless, K^+ could be transported in
515 such limiting conditions by other unknown transporters. Several putative transporters
516 were identified as essential and high fitness cost in our Tn-seq analysis (i.e
517 CCNA_01159 and CCNA_00494) and up-regulated in the RNA-seq analysis (i.e
518 CCNA_00339, CCNA_01852, CCNA_01587, CCNA_01588 CCNA_02570,
519 CCNA_02571, …). It is possible that one or several of them assist the activity of
520 KdpABC in limiting K^+.

521 As in *E. coli*, the expression of *kdp* operon in *C. crescentus* is activated upon K^+
522 starvation by the KdpDE TCS (Polarek *et al.*, 1992). However, we found surprising
523 differences since in the absence of the histidine kinase (HK) KdpD, (i) *kdp* is still
524 expressed, although to a lesser extent than in WT cells and (ii) the *kdp* promoter (P_{kdp})
525 is more active in stationary phase. Our genetic dissection of the catalytic activity of
526 KdpDE with point mutants in *kdpE* (phospho-mimetic $kdpE_{D56E}$ and phospho-ablative
527 $kdpE_{D56A}$) and KdpD (K^-/P^- $kdpD_{H670N}$ and K^-/P^+ $kdpD_{F832L}$) strongly suggest that (i)
528 KdpE can be phosphorylated by another – non-cognate – HK, at least in the absence
529 of KdpD and that (ii) KdpD switches mainly to a phosphatase in late exponential phase
530 of growth.

531 In *E. coli*, deletion of the *kdpD* results in a prominent growth arrest, of more than 20
532 hours, before restarting growth thanks to KdpE phosphorylation by PhoR. However, it
533 never surpassed the WT plateau as seen with *C. crescentus* Δ*kdpD*, $kdpD_{H670N}$ and
534 $kdpE_{D56E}$ mutants. Thus, the higher plateau is due to the loss of KdpD phosphatase
535 activity. The KdpD phosphatase activity has be shown to be stimulated by intracellular
536 K^+ intracellular levels (Schramke *et al.*, 2016). Four amino acids located in the second

537 periplasmic loop were identified as an extracellular K^+-specific recognition site. Hence,
538 substitution of those four amino acids by alanine resulted in a strain unable to sense
539 extracellular K^+. In contrast, the K^+-recognition site for intracellular sensing remains to
540 be identified. However, although specific residues could not be highlighted, the C-
541 terminal cytoplasmic domain of KdpD was described to display a K^+-dependent
542 phosphatase activity (Cann, 2007, Dani *et al.*, 2017). Although this has yet to be
543 experimentally investigated, authors suggested that the cytoplasmic GAF domain of
544 KdpD may be responsible for intracellular K^+ sensing. Most GAF domains are involved
545 in regulatory functions through binding to cyclic nucleotides or other small ligands
546 including ions (Cann, 2007, Heikaus *et al.*, 2009). Interestingly, we found that KdpD
547 from *C. crescentus* lacks a GAF domain. Therefore, it is possible that such a
548 connection between intracellular sensing and phosphatase activity does not exist in *C.*
549 *crescentus*, which would explain why KdpD mainly acts as a phosphatase.

550 As mentioned above, in *E. coli*, the HK PhoR can crosstalk with the RR KdpE, which
551 allows a Δ*kdpD* mutant to grow in a low K^+ environment after a long lag phase
552 (Schramke *et al.*, 2017) . Since PhoR is conserved in *C. crescentus*, it constitutes a
553 good candidate for the non-cognate HK phosphorylating KdpE. To test this hypothesis,
554 we could measure growth behaviour as well as P_{kdp} activity in a strain in which both
555 *kdpD* and *phoR* were inactivated. PhoR is a sensor kinase regulating the
556 phosphorylation levels and activity of the RR PhoB, which drives the Pho regulon, that
557 is the entire set of genes whose expression relies on phosphate availability.
558 Interestingly, a crosstalk between KdpD and PhoB was also described, which means
559 that in the absence of PhoR, PhoB can be phosphorylated by KdpD in low phosphate
560 conditions (Schramke *et al.*, 2017) . The double crosstalk suggests there is tight

561 connection between K^+ and phosphate homeostasis. Since both TCS – KdpDE and
562 PhoBR – are conserved in *C. crescentus*, it could be worth testing if the crosstalk exists
563 in both directions as well.

564 Interestingly, we observed that Kup activity varies in excessive concentrations
565 depending on the media. This indicates that Kup activity is regulated in toxic K^+
566 concentrations depending on environmental resources and/or metabolic states. Also,
567 suppressor mutations that bypass the growth defect of Δ*kdp* cells in limiting K^+
568 conditions have been mapped in *kup* without impacting the growth when K^+ was
569 available. A plausible explanation would be that mutations found in Kup increase its
570 affinity for K^+, thereby increasing K^+ transport to compensate the loss of Kdp, and that
571 the efflux systems (KefB and KefC) limits the intracellular K^+ concentration in abundant
572 K^+ conditions. Studies in other bacteria indicate Kup is a single membrane protein
573 showing moderate affinity for K^+ (Rhoads *et al.*, 1976, Sato *et al.*, 2014). In
574 *Lactococcus lactis,* the second messenger c-di-AMP binds to Kup homologues, in
575 addition to the Trk homologue, to inhibit K^+ transport (Quintana *et al.*, 2019). It is
576 therefore possible that Kup activity is regulated by intracellular signalling molecules to
577 coordinate K^+ uptake with environmental conditions.

578 KdpD homologues have also been reported to bind to c-di-AMP in other Gram-positive
579 bacteria (Dutta *et al.*, 2021, Moscoso *et al.*, 2016). High levels of c-di-AMP inhibit the
580 KdpD-dependent upregulation of the *kdp* operon in *Staphylococcus aureus* (Moscoso
581 *et al.*, 2016). On top of this, genes encoding K^+ transporters are also regulated by a c-
582 di-AMP-dependent riboswitch. The 5' leader region (LR) of the *B. subtilis kimA*
583 transcript can adopt two mutually exclusive conformations, one favouring transcription
584 readthrough while the other promoting transcription termination (Nelson *et al.*, 2013).

585 Upon direct binding of c-di-AMP, the *kimA* 5' LR preferentially forms a structure
586 exposing a predicted intrinsic transcription terminator, thereby inhibiting transcription
587 elongation of *kimA*. Interestingly, a study showed that transcription levels of *kimA* were
588 higher in low K^+ conditions (0.1 mM KCl) than at higher K^+ concentrations (5 mM KCl)
589 (Gundlach *et al.*, 2017). Indeed, the high-affinity K^+ transporter KimA was exclusively
590 detected in low K^+ conditions. This K^+-dependent control of *kimA* expression is
591 suggested to be achieved through a modulation of c-di-AMP intracellular levels.
592 Supporting this hypothesis, concentrations of c-di-AMP were increased by two-fold in
593 high K^+ conditions. More than just increasing in concentration, c-di-AMP becomes
594 indispensable in high K^+ conditions since a strain lacking c-di-AMP synthesising genes
595 is viable at low but not at high K^+ concentrations. *C. crescentus* produces c-di-GMP,
596 rather than c-di-AMP, to control cell development and division. If we speculate that c-
597 di-GMP levels fluctuate reminiscently to that of c-di-AMP, K^+-depletion would result in
598 low c-di-GMP levels thereby preventing progression in cell cycle. Although it remains
599 unclear how K^+ limitation leads to a decrease in c-di-AMP levels, it has been shown
600 that the enzymes producing c-di-AMP in *B. subtilis* were less abundant in low K^+
601 conditions (Gundlach *et al.*, 2017). Evaluating the growth behaviour of cells unable to
602 synthesize c-di-GMP (Abel *et al.*, 2013) in excessive or limiting K^+ conditions could be
603 an initial step to assess if such regulation is conserved.

604 The nitrogen-related phosphotransferase component $EIIA^{Ntr}$ has been shown in *E. coli*
605 to regulate not only K^+ transport, by modulating KdpD kinase activity (Luttmann *et al.*,
606 2015, Mork-Morkenstein *et al.*, 2017, Zimmer *et al.*, 2008) but also phosphate
607 starvation response, by modulating PhoR activity (Luttmann *et al.*, 2012). For instance,
608 in limiting K^+ conditions (< 5 mM), the unphosphorylated form of $EIIA^{Ntr}$ was shown to

609 directly interact with KdpD and stimulate its kinase activity, thereby promoting
610 phosphorylation of KdpE and the subsequent increase of *kdp* genes expression
611 (Luttmann *et al.*, 2009). This $EIIA^{Ntr}$-based control of KdpD has also been reported in
612 the plant symbionts *Rhizobium leguminosarum* (Untiet *et al.*, 2013) and *Sinorhizobium*
613 *fredii* (Feng *et al.*, 2022), two α-proteobacteria closely related to *C. crescentus*. It was
614 later discovered that $EIIA^{Ntr}$ regulates in fact sigma factor selectivity by modulating K^+
615 levels. Indeed, the competition between σ^{70} and σ^S for interaction with the RNA
616 polymerase (RNAP) is influenced by K^+ intracellular levels (Lee *et al.*, 2010).
617 Depending on the phosphorylation state of $EIIA^{Ntr}$, the resulting K^+ intracellular levels
618 preferentially favour the binding of either σ^{70} or σ^S to the core RNAP (Lee *et al.*, 2010).
619 Interestingly, PTS^{Ntr} components regulate the levels of another signalling molecule –
620 (p)ppGpp – that connects cell division with environmental and metabolic cues in *C.*
621 *crescentus* (Hallez *et al.*, 2017, Ronneau *et al.*, 2016, Shyp *et al.*, 2021). Knowing that
622 (p)ppGpp also influences gene expression by regulating sigma factor competition
623 (Jishage *et al.*, 2002), it is therefore tempting to speculate that $EIIA^{Ntr}$ and/or (p)ppGpp
624 participate to the K^+ homeostasis in *C. crescentus*, even in other alphaproteobacteria.

625 We also generated strains in which either *kefB* or *kefC* – both coding for efflux pumps
626 – was inactivated. We observed that deletion of *kefC* (Δ*kefC*) dramatically impaired
627 growth in excess of K^+, while the *kefB* mutant (Δ*kefB*) behaved like the WT strain,
628 suggesting that KefB cannot support KefC functions. Recently, it was reported that
629 glutathione controls cell division via negative regulation of the potassium (K^+) efflux
630 pump KefB (Hartl *et al.*, 2020). Indeed, cell filamentation and decreased intracellular
631 K^+ levels were observed in mutants unable to synthesize glutathione (Δ*gshB*),
632 suggesting that K^+ homeostasis is crucial for bacterial cell cycle regulation.

633 Interestingly, mutations that suppressed Δ*gshB* phenotypes were found in *kefB* and
634 *kefG*, but not in *kefC*. This indicated that, glutathione regulation in *C. crescentus* occurs
635 mainly through *kefB*. Therefore, it is likely that the glutathione-dependent negative
636 regulation on KefB still occurred in Δ*kefC* cells, which would explain why the single
637 *kefC* knock-out mutant failed to grow when K^+ was in excess whereas the single Δ*kefC*
638 grew.

639

640 # Methods

641 **Bacterial strains and growth conditions.**

642 All *Escherichia coli* strains used in this thesis were grown aerobically in Luria-Bertani
643 (LB) broth (Sigma). *E. coli* Top10 was used for cloning purpose while *E. coli* MT607
644 was used for triparental matings. Thermo-competent cells were used for transformation
645 of *E. coli*. All *Caulobacter crescentus* strains used are derived from the synchronizable
646 wild-type strain NA1000. The traditional synthetic media supplemented with glucose
647 (M2G) was modified by replacing potassium salts by their equivalent sodium salts to
648 obtain a medium without any K^+ (K_0) to which the desired K^+ concentrations could be
649 added. The source of K^+ consists in both KH_2PO_4 and K_2HPO_4 mixed to an equivalent
650 ratio in terms of K^+ concentration. For each experiment, cells were first grown at 30 °C;
651 in Peptone Yeast Extract (PYE), then adapted overnight at 30 °C in K_0 media
652 supplemented with 0.5 mM K^+, washed twice in K_0 media and finally grown at 30 °C in
653 K_0 media supplemented with the desired K^+ concentration. For growth curve
654 measurements, cultures were diluted to a final OD_{660} of 0.02 in a 96-well plate. Growth
655 was monitored during 48 h with continuous shaking at 30 °C, in an automated plate

656 reader (Bioscreen C, Lab Systems) measuring OD_{660} every 10 min. For *E. coli*,
657 antibiotics were used at the following concentrations (μg/ml; in liquid/solid medium):
658 chloramphenicol (20/30), kanamycin (30/50), oxytetracycline (12.5/12.5),
659 spectinomycin (100/100), streptomycin (50/100) while for *C. crescentus*, media were
660 supplemented with kanamycin (5/20), oxytetracycline (2.5/2.5), nalidixic acid (20) when
661 appropriate. Genes under the control of the inducible xylose promoter (P_{xylX}) were
662 induced with 0.1 % xylose. Plasmid delivery into *C. crescentus* was achieved by either
663 bi- or tri-parental mating using *E. coli* S17-1 and *E. coli* MT607 as helper strains,
664 respectively. In-frame deletions were created by using the pNPTS138-derivative
665 plasmids as follows. Integration of the plasmids in the *C. crescentus* genome after
666 single homologous recombination were selected on PYE plates supplemented with
667 kanamycin. Three independent recombinant clones were inoculated in PYE medium
668 without kanamycin and incubated overnight at 30 °C. Then, dilutions were spread on
669 PYE plates supplemented with 3% sucrose and incubated at 30 °C. Single colonies
670 were picked and transferred onto PYE plates with and without kanamycin. Finally, to
671 discriminate between mutated and wild-type loci, kanamycin-sensitive clones were
672 tested by PCR on colony using locus-specific oligonucleotides.

673 **Spotting assays**

674 Ten-fold serial dilutions (in M2G-K) were prepared in 96-well plates from 5 ml cultures
675 in standard universal tubes grown overnight at 30 °C in the corresponding media. Cells
676 (5μl) were then spotted on plates, incubated at 30 °C for two-to-three days and pictures
677 were taken.

678 **β-galactosidase assays**

679 β-galactosidase assays were performed as already described in (Quintero-Yanes *et*
680 *al.*, 2022). Briefly, cultures were either grown to stationary phase directly in a 96-wells
681 plate or grown in flasks from which samples were withdrawn throughout growth and
682 placed at -80 °C in between time points. Permeabilization of cells was performed by
683 incubating cells with lysis buffer (20 mg/ml polymyxin B, β-mercaptoethanol) for 30 min
684 at 28 °C. Then, 50 μl of 4 mg/ml O-nitrophenyl- β-D-galactopyranoside (ONPG) were
685 added. Lysis and ONPG solutions were prepared using Z buffer as a solvent (60 mM
686 Na_2HPO_4, 40 mM NaH_2PO_4, 10 mM KCl, 1 mM $MgSO_4$, pH 7.0). Both OD_{420} and OD_{550}
687 were measured every minute for 30 min at 30 °C using a fluorimeter (SpectraMax®,
688 Molecular Devices). Miller Units were calculated using the following formula: M.U. =
689 $\frac{[OD420 - (1.75\ x\ OD550)]x\ 1000}{OD660x\ t\ x\ v}$ where t is the reaction time in min v is the volume of culture
690 used in ml. Then, ONPG hydrolysis was measured at 30 °C for 30 min. The activity of
691 the β-galactosidase expressed in miller units (MU) was calculated using the following
692 equation: MU = (OD_{420} × 1,000) / [OD_{660} × t × v] where "t" is the time of the reaction
693 (min), and "v" is the volume of cultures used in the assays (ml). Experimental values
694 were the average of three independent experiments.

695 **Protein purification and production of polyclonal antibodies**

696 To immunize rabbits for production of polyclonal antibodies, an *E. coli* BL21 (DE3)
697 pLysS strain carrying plasmid pET-28a-*kdpE* was grown in LB medium supplemented
698 with kanamycin and chloramphenicol until an OD600 of 0.5. After addition of IPTG to
699 a final concentration of 1 mM, the culture was incubated at 18 °C for 18 hrs. Cells were
700 then harvested by centrifugation for 30 min at 5,000 x g, 4 °C. The pellet was
701 resuspended in 20 ml of binding buffer (20 mM Tris-HCl pH 8.0, 500 mM NaCl, 10%
702 glycerol, 10 mM $MgCl_2$, 12.5 mM Imidazole) supplemented with complete EDTA-free

703 protease cocktail inhibitor (Roche), 400 mg lysozyme (Sigma) and 10 mg DNaseI
704 (Roche) and incubated for 30 min on ice. Cells were then lysed by sonication. After
705 centrifugation at 12,000 rpm for 30 min at 4°C, the lysate was loaded on a Ni-NTA
706 column and incubated 1 hr at 4 °C with end-over-end agitation. The column was then
707 washed with 5 ml binding buffer, 3 ml Wash1 buffer (binding buffer with 25 mM
708 imidazole), 3 ml Wash2 buffer (binding buffer with 50 mM imidazole), 3 ml Wash3
709 buffer (binding buffer with 75 mM imidazole). Proteins bound to the column were eluted
710 with 3 ml Elution buffer (binding buffer with 100 mM imidazole) and aliquoted in 300 μl
711 fractions. All the fractions containing the protein of interest (checked by Coomassie
712 blue staining) were pooled and dialyzed in Dialysis buffer (20 mM Tris pH 8, 500 mM
713 NaCl, 10% glycerol). Purified KdpE was used to immunize rabbits (CER Groupe,
714 Marloie, Belgium).

715 **Tn-seq analysis.**

716 A mini-Tn5 was introduced in *C. crescentus* NA1000 WT strain by bi-parental mating.
717 Briefly, overnight cultures of recipient and donor strains (grown in LB supplemented
718 with kanamycin) were mixed in 95:5 ratio to a final volume of 1 ml. Cells were harvested
719 by centrifugation at 9,000 rpm (7,600 x g) at room temperature for 2 min. The
720 supernatant was removed, and 1 ml of fresh PYE medium was added to wash the
721 pellet. A second centrifugation step was done to remove again the supernatant.
722 Thereafter, the pellet was resuspended in 50 μl and spotted on PYE agar and
723 incubated at 30 ° C for 4h. Cells were collected, resuspended in 10 ml M2G or M2G-K
724 and washed twice with the same volume. Dilutions (10^{-6}) were plated on M2G or M2G-
725 K plates supplemented with aztreonam (5μg l^{-1}) and kanamycin (5μg l^{-1}) and incubated
726 at 30 ° C for 5 days. Then, at least 3 x10^5 colonies were collected in M2G or M2G-K

727 supplemented with 10% glycerol and stored at -80 °C. Genomic DNA was then
728 extracted following the *Nucleospin Tissue Kit* protocol (Macherey-Nagel) and
729 resuspended in 50 μl elution buffer (5 mM Tris-HCl [pH 8.5]). DNA sequencing was
730 performed using an Illumina NextSeq (paired-end 2x75) instrument (Fasteris, Geneva,
731 Switzerland). Reads corresponding to the mini-Tn5 insertion sites were first filtered
732 with the 5'-GGTTGAGATGTGTATAAGAGACAG sequence before being processed as
733 described in (Coppine *et al.*, 2020). Briefly, filtered reads were mapped on the genome
734 of *C. crescentus* NA1000 (GenBank accession number NC_011916.1) and converted
735 to Sequence Alignment/Map (SAM) format using the Burrows-Wheeler Aligner (BWA)
736 and SAMtools, respectively, from the Sourceforge server (https://sourceforge.net/).
737 Next, the number of reads overlapping each genomic position was computed using
738 custom Python scripts. The total number of reads for internal 80% of each ORF in each
739 condition were then computed using custom Python scripts. For comparing strains, the
740 total number of reads was normalized by the ratio of the number of reads between the
741 two strains. Ward's clustering analysis was performed to define the fitness categories
742 as previously reported.

743 **Chromatin immunoprecipitation followed by deep sequencing (ChIP-Seq assay)**

744 ChIP-Seq was performed as already described in (Coppine *et al.*, 2020). Briefly, 80 ml
745 of mid-log-phase cells (OD_{660} of 0.6) were cross-linked in 1% formaldehyde and 10
746 mM sodium phosphate (pH 7.6) at room temperature (RT) for 10 min and then for 30
747 min on ice. Cross-linking was stopped by addition of 125 mM glycine and incubated for
748 5 min on ice. Cells were washed twice in phosphate buffer solution (PBS; 137 mM
749 NaCl, 2.7 mM KCl, 10 mM Na_2HPO_4, 1.8 mM KH_2PO_4, pH 7.4) resuspended in 450 μl
750 TES buffer (10 mM Tris-HCl [pH 7.5], 1 mM EDTA, and 100 mM NaCl), and lysed with

751 2 μl of Ready-lyse lysozyme solution for 5 min at RT. Protease inhibitors (Roche) were
752 added, and the mixture was incubated for 10 min. Then, 550 μl of ChIP buffer (1.1%
753 Triton X-100, 1.2 mM EDTA, 16.7 mM Tris-HCl [pH 8.1], 167 mM NaCl, protease
754 inhibitors) were added to the lysate and incubated at 37 °C for 10 min before sonication
755 (2 x 8 bursts of 30 sec on ice using a Diagenode Bioruptor) to shear DNA fragments
756 to a length of 300 to 500 bp. Lysate was cleared by centrifugation for 10 min at 12,500
757 rpm at 4 °C, and protein content was assessed by measuring the OD_{280}. Then, 7.5 mg
758 of proteins was diluted in ChIP buffer supplemented with 0.01% SDS and precleared
759 for 1 hr at 4 °C with 50 μl of SureBeads Protein A Magnetic Beads (BioRad) and 100
760 μg bovine serum albumin (BSA). One microliter of polyclonal anti-KdpE antibodies was
761 added to the supernatant before overnight incubation at 4 °C under gentle agitation.
762 Next, 80 μl of BSA presaturated protein A-agarose beads were added to the solution
763 and incubated for 2 hrs at 4 °C with rotation, washed once with low-salt buffer (0.1%
764 SDS, 1% Triton X-100, 2 mM EDTA, 20 mM Tris-HCl [pH 8.1], 150 mM NaCl), once
765 with high-salt buffer (0.1% SDS, 1% Triton X-100, 2 mM EDTA, 20 mM Tris-HCl [pH
766 8.1], 500 mM NaCl), once with LiCl buffer (0.25 M LiCl, 1% NP-40, 1% deoxycholate,
767 1 mM EDTA, 10 mM Tris-HCl [pH 8.1]), and once with TE buffer (10 mM Tris-HCl [pH
768 8.1] 1 mM EDTA) at 4 °C, followed by a second wash with TE buffer at RT. The DNA-
769 protein complexes were eluted twice in 250 μl freshly prepared elution buffer (0.1 M
770 NaHCO3, 1% SDS). NaCl was added at a concentration of 300 mM to the combined
771 eluates (500 μl) before overnight incubation at 65 °C to reverse the cross-link. The
772 samples were treated with 20 μg of proteinase K in 40mM EDTA and 40 mM Tris-HCl
773 (pH 6.5) for 2 h at 45 °C. DNA was extracted using a Nucleospin PCR cleanup kit
774 (Macherey-Nagel) and resuspended in 50 μl elution buffer (5 mM Tris-HCl [pH 8.5]).

775 DNA sequencing was performed using an Illumina NextSeq 550 (paired-end 2x75)
776 instrument (Seqalis). NGS data were analysed as described in (Coppine *et al.*, 2020).

777 **RNA-Seq**

778 WT and Δ*kdpE* cells were grown overnight to OD_{660} ~ 0.3 in M2G-K 0,025 mM K^+ and
779 WT in M2G-K 0,5 mM K^+. Thereafter, total RNA was extracted with RNeasy® Protect
780 Bacteria Kit from Qiagen and following manufacturer's instructions. The quantity and
781 quality (A260/A280 ration) of RNA was determined with a Thermo Scientific™
782 Nanodrop ™ One Microvolume UV-Vis Spectrophotometer. RNA-Seq TTRNA libraries
783 were prepared according to the manufacturer's instructions and sequenced with
784 Illumina NovaSeq 6000 (paired-end 2x100) instrument (Seqalis). NGS data were
785 analysed using Galaxy (https://usegalaxy.org) (Quintero-Yanes *et al.*, 2022). Briefly,
786 FastQC was used to evaluate the quality of the reads; HISAT2 was used to map the
787 reads onto the NA1000 reference genome (NC_011916.1) and generate bam files;
788 featureCounts was used to generate counts tables using bam files and DESeq2 was
789 used to determine differentially expressed genes. The Volcano plot was generated
790 using GraphPad Prism 9 software.

791 **MEME analysis**

792 Sequences corresponding to the peaks founds in ChIP-seq were analysed for a KdpE
793 conserved DNA binding motif using MEME (Quintero-Yanes *et al.*, 2022) (**Table S6**).
794 As searching parameters, the classical motif discovery mode, zoops motif site
795 distribution, 10 minimum motif width and 20 maximum motif width, 2 as maximum
796 number of motifs and a p-value<0.001 as cut-off were used. The motif with highest site
797 count was selected.

798 **Statistical analyses**

799 All the statistical analyses were performed using GraphPad Prism 9 software. A *P*
800 value of <0.05 was considered as significant.

801 **Data availability**

802 ChIP-Seq and RNA-Seq data have been deposited to the Gene Expression Omnibus
803 (GEO) repository with the accession number XXX.

804 ## References

805 Abel, S., Bucher, T., Nicollier, M., Hug, I., Kaever, V., Abel Zur Wiesch, P., and Jenal, U. (2013)
806 Bi-modal distribution of the second messenger c-di-GMP controls cell fate and
807 asymmetry during the caulobacter cell cycle. *PLoS Genet* **9**: e1003744.
808 Ahijado-Guzman, R., Alfonso, C., Reija, B., Salvarelli, E., Mingorance, J., Zorrilla, S., Monterroso,
809 B., and Rivas, G. (2013) Control by potassium of the size distribution of Escherichia coli
810 FtsZ polymers is independent of GTPase activity. *J Biol Chem* **288**: 27358-27365.
811 Ali, M.K., Li, X., Tang, Q., Liu, X., Chen, F., Xiao, J., Ali, M., Chou, S.H., and He, J. (2017)
812 Regulation of Inducible Potassium Transporter KdpFABC by the KdpD/KdpE Two-
813 Component System in Mycobacterium smegmatis. *Front Microbiol* **8**: 570.
814 Bakker, E.P., and Mangerich, W.E. (1981) Interconversion of components of the bacterial
815 proton motive force by electrogenic potassium transport. *J Bacteriol* **147**: 820-826.
816 Booth, I.R. (1999) The regulation of intracellular pH in bacteria. *Novartis Found Symp* **221**: 19-
817 28; discussions 28-37.
818 Bossemeyer, D., Borchard, A., Dosch, D.C., Helmer, G.C., Epstein, W., Booth, I.R., and Bakker,
819 E.P. (1989a) K+-transport protein TrkA of Escherichia coli is a peripheral membrane
820 protein that requires other trk gene products for attachment to the cytoplasmic
821 membrane. *J Biol Chem* **264**: 16403-16410.
822 Bossemeyer, D., Schlosser, A., and Bakker, E.P. (1989b) Specific cesium transport via the
823 Escherichia coli Kup (TrkD) K+ uptake system. *J Bacteriol* **171**: 2219-2221.
824 Cann, M. (2007) A subset of GAF domains are evolutionarily conserved sodium sensors. *Mol*
825 *Microbiol* **64**: 461-472.
826 Cao, Y., Jin, X., Huang, H., Derebe, M.G., Levin, E.J., Kabaleeswaran, V., Pan, Y., Punta, M., Love,
827 J., Weng, J., Quick, M., Ye, S., Kloss, B., Bruni, R., Martinez-Hackert, E., Hendrickson,
828 W.A., Rost, B., Javitch, J.A., Rajashankar, K.R., Jiang, Y., and Zhou, M. (2011) Crystal
829 structure of a potassium ion transporter, TrkH. *Nature* **471**: 336-340.
830 Castaneda-Garcia, A., Do, T.T., and Blazquez, J. (2011) The K+ uptake regulator TrkA controls
831 membrane potential, pH homeostasis and multidrug susceptibility in Mycobacterium
832 smegmatis. *J Antimicrob Chemother* **66**: 1489-1498.
833 Coppine, J., Kaczmarczyk, A., Petit, K., Brochier, T., Jenal, U., and Hallez, R. (2020) Regulation
834 of Bacterial Cell Cycle Progression by Redundant Phosphatases. *J Bacteriol* **202**.

835 Curtis, P.D., and Brun, Y.V. (2014) Identification of essential alphaproteobacterial genes
836 reveals operational variability in conserved developmental and cell cycle systems. *Mol*
837 *Microbiol* **93**: 713-735.
838 Danchin, A., and Nikel, P.I. (2019) Why Nature Chose Potassium. *J Mol Evol* **87**: 271-288.
839 Dani, P., Ujaoney, A.K., Apte, S.K., and Basu, B. (2017) Regulation of potassium dependent
840 ATPase (kdp) operon of Deinococcus radiodurans. *PLoS One* **12**: e0188998.
841 de Oliveira, M.V., Intorne, A.C., Vespoli, L.S., Andrade, L.F., Pereira, L.M., Rangel, P.L., and de
842 Souza Filho, G.A. (2017) Essential role of K(+) uptake permease (Kup) for resistance to
843 sucrose-induced stress in Gluconacetobacter diazotrophicus PAl 5. *Environ Microbiol*
844 *Rep* **9**: 85-90.
845 Dominguez-Ferreras, A., Munoz, S., Olivares, J., Soto, M.J., and Sanjuan, J. (2009) Role of
846 potassium uptake systems in Sinorhizobium meliloti osmoadaptation and symbiotic
847 performance. *J Bacteriol* **191**: 2133-2143.
848 Dosch, D.C., Helmer, G.L., Sutton, S.H., Salvacion, F.F., and Epstein, W. (1991) Genetic analysis
849 of potassium transport loci in Escherichia coli: evidence for three constitutive systems
850 mediating uptake potassium. *J Bacteriol* **173**: 687-696.
851 Dutta, A., Batish, M., and Parashar, V. (2021) Structural basis of KdpD histidine kinase binding
852 to the second messenger c-di-AMP. *J Biol Chem* **296**: 100771.
853 Epstein, W. (2003) The roles and regulation of potassium in bacteria. *Prog Nucleic Acid Res*
854 *Mol Biol* **75**: 293-320.
855 Feifel, B., Sandmeier, E., Schonfeld, H.J., and Christen, P. (1996) Potassium ions and the
856 molecular-chaperone activity of DnaK. *Eur J Biochem* **237**: 318-321.
857 Feng, X.Y., Tian, Y., Cui, W.J., Li, Y.Z., Wang, D., Liu, Y., Jiao, J., Chen, W.X., and Tian, C.F. (2022)
858 The PTS(Ntr)-KdpDE-KdpFABC Pathway Contributes to Low Potassium Stress
859 Adaptation and Competitive Nodulation of Sinorhizobium fredii. *mBio* **13**: e0372121.
860 Gohara, D.W., and Di Cera, E. (2016) Molecular Mechanisms of Enzyme Activation by
861 Monovalent Cations. *J Biol Chem* **291**: 20840-20848.
862 Grason, J.P., Gresham, J.S., Widjaja, L., Wehri, S.C., and Lorimer, G.H. (2008) Setting the
863 chaperonin timer: the effects of K+ and substrate protein on ATP hydrolysis. *Proc Natl*
864 *Acad Sci U S A* **105**: 17334-17338.
865 Gries, C.M., Bose, J.L., Nuxoll, A.S., Fey, P.D., and Bayles, K.W. (2013) The Ktr potassium
866 transport system in Staphylococcus aureus and its role in cell physiology, antimicrobial
867 resistance and pathogenesis. *Mol Microbiol* **89**: 760-773.
868 Gubaev, A., and Klostermeier, D. (2012) Potassium ions are required for nucleotide-induced
869 closure of gyrase N-gate. *J Biol Chem* **287**: 10916-10921.
870 Gundlach, J., Herzberg, C., Kaever, V., Gunka, K., Hoffmann, T., Weiss, M., Gibhardt, J.,
871 Thurmer, A., Hertel, D., Daniel, R., Bremer, E., Commichau, F.M., and Stulke, J. (2017)
872 Control of potassium homeostasis is an essential function of the second messenger
873 cyclic di-AMP in Bacillus subtilis. *Sci Signal* **10**.
874 Hallez, R., Delaby, M., Sanselicio, S., and Viollier, P.H. (2017) Hit the right spots: cell cycle
875 control by phosphorylated guanosines in alphaproteobacteria. *Nat Rev Microbiol* **15**:
876 137-148.
877 Harms, C., Domoto, Y., Celik, C., Rahe, E., Stumpe, S., Schmid, R., Nakamura, T., and Bakker,
878 E.P. (2001) Identification of the ABC protein SapD as the subunit that confers ATP
879 dependence to the K+-uptake systems Trk(H) and Trk(G) from Escherichia coli K-12.
880 *Microbiology (Reading)* **147**: 2991-3003.

881 Hartl, J., Kiefer, P., Kaczmarczyk, A., Mittelviefhaus, M., Meyer, F., Vonderach, T., Hattendorf,
882 B., Jenal, U., and Vorholt, J.A. (2020) Untargeted metabolomics links glutathione to
883 bacterial cell cycle progression. *Nat Metab* **2**: 153-166.
884 Heermann, R., and Jung, K. (2010) The complexity of the 'simple' two-component system
885 KdpD/KdpE in Escherichia coli. *FEMS Microbiol Lett* **304**: 97-106.
886 Heikaus, C.C., Pandit, J., and Klevit, R.E. (2009) Cyclic nucleotide binding GAF domains from
887 phosphodiesterases: structural and mechanistic insights. *Structure* **17**: 1551-1557.
888 Hocking, J., Priyadarshini, R., Takacs, C.N., Costa, T., Dye, N.A., Shapiro, L., Vollmer, W., and
889 Jacobs-Wagner, C. (2012) Osmolality-dependent relocation of penicillin-binding
890 protein PBP2 to the division site in Caulobacter crescentus. *J Bacteriol* **194**: 3116-3127.
891 Humphries, J., Xiong, L., Liu, J., Prindle, A., Yuan, F., Arjes, H.A., Tsimring, L., and Suel, G.M.
892 (2017) Species-Independent Attraction to Biofilms through Electrical Signaling. *Cell*
893 **168**: 200-209 e212.
894 Jishage, M., Kvint, K., Shingler, V., and Nystrom, T. (2002) Regulation of sigma factor
895 competition by the alarmone ppGpp. *Genes Dev* **16**: 1260-1270.
896 Karp, P.D., Billington, R., Caspi, R., Fulcher, C.A., Latendresse, M., Kothari, A., Keseler, I.M.,
897 Krummenacker, M., Midford, P.E., Ong, Q., Ong, W.K., Paley, S.M., and Subhraveti, P.
898 (2019) The BioCyc collection of microbial genomes and metabolic pathways. *Brief*
899 *Bioinform* **20**: 1085-1093.
900 Klenow, H., and Henningsen, I. (1969) Effect of monovalent cations on the activity of the DNA
901 polymerase of Escherichia coli B. *Eur J Biochem* **9**: 133-141.
902 Laimins, L.A., Rhoads, D.B., and Epstein, W. (1981) Osmotic control of kdp operon expression
903 in Escherichia coli. *Proc Natl Acad Sci U S A* **78**: 464-468.
904 Lee, C.R., Cho, S.H., Kim, H.J., Kim, M., Peterkofsky, A., and Seok, Y.J. (2010) Potassium
905 mediates Escherichia coli enzyme IIA(Ntr) -dependent regulation of sigma factor
906 selectivity. *Mol Microbiol* **78**: 1468-1483.
907 Liu, L.F., and Wang, J.C. (1978) Micrococcus luteus DNA gyrase: active components and a
908 model for its supercoiling of DNA. *Proc Natl Acad Sci U S A* **75**: 2098-2102.
909 Liu, Y., Ho, K.K., Su, J., Gong, H., Chang, A.C., and Lu, S. (2013) Potassium transport of
910 Salmonella is important for type III secretion and pathogenesis. *Microbiology*
911 *(Reading)* **159**: 1705-1719.
912 Luttmann, D., Gopel, Y., and Gorke, B. (2012) The phosphotransferase protein EIIA(Ntr)
913 modulates the phosphate starvation response through interaction with histidine
914 kinase PhoR in Escherichia coli. *Mol Microbiol* **86**: 96-110.
915 Luttmann, D., Gopel, Y., and Gorke, B. (2015) Cross-Talk between the Canonical and the
916 Nitrogen-Related Phosphotransferase Systems Modulates Synthesis of the KdpFABC
917 Potassium Transporter in Escherichia coli. *J Mol Microbiol Biotechnol* **25**: 168-177.
918 Luttmann, D., Heermann, R., Zimmer, B., Hillmann, A., Rampp, I.S., Jung, K., and Gorke, B.
919 (2009) Stimulation of the potassium sensor KdpD kinase activity by interaction with
920 the phosphotransferase protein IIA(Ntr) in Escherichia coli. *Mol Microbiol* **72**: 978-994.
921 MacGilvary, N.J., Kevorkian, Y.L., and Tan, S. (2019) Potassium response and homeostasis in
922 Mycobacterium tuberculosis modulates environmental adaptation and is important
923 for host colonization. *PLoS Pathog* **15**: e1007591.
924 Matroule, J.Y., Lam, H., Burnette, D.T., and Jacobs-Wagner, C. (2004) Cytokinesis monitoring
925 during development; rapid pole-to-pole shuttling of a signaling protein by localized
926 kinase and phosphatase in Caulobacter. *Cell* **118**: 579-590.

927 Mork-Morkenstein, M., Heermann, R., Gopel, Y., Jung, K., and Gorke, B. (2017) Non-canonical
928 activation of histidine kinase KdpD by phosphotransferase protein PtsN through
929 interaction with the transmitter domain. *Mol Microbiol* **106**: 54-73.
930 Moscoso, J.A., Schramke, H., Zhang, Y., Tosi, T., Dehbi, A., Jung, K., and Grundling, A. (2016)
931 Binding of Cyclic Di-AMP to the Staphylococcus aureus Sensor Kinase KdpD Occurs via
932 the Universal Stress Protein Domain and Downregulates the Expression of the Kdp
933 Potassium Transporter. *J Bacteriol* **198**: 98-110.
934 Nelson, J.W., Sudarsan, N., Furukawa, K., Weinberg, Z., Wang, J.X., and Breaker, R.R. (2013)
935 Riboswitches in eubacteria sense the second messenger c-di-AMP. *Nat Chem Biol* **9**:
936 834-839.
937 Ochrombel, I., Ott, L., Kramer, R., Burkovski, A., and Marin, K. (2011) Impact of improved
938 potassium accumulation on pH homeostasis, membrane potential adjustment and
939 survival of Corynebacterium glutamicum. *Biochim Biophys Acta* **1807**: 444-450.
940 Pedersen, B.P., Stokes, D.L., and Apell, H.J. (2019) The KdpFABC complex - K(+) transport
941 against all odds. *Mol Membr Biol* **35**: 21-38.
942 Polarek, J.W., Williams, G., and Epstein, W. (1992) The products of the kdpDE operon are
943 required for expression of the Kdp ATPase of Escherichia coli. *J Bacteriol* **174**: 2145-
944 2151.
945 Prindle, A., Liu, J., Asally, M., Ly, S., Garcia-Ojalvo, J., and Suel, G.M. (2015) Ion channels enable
946 electrical communication in bacterial communities. *Nature* **527**: 59-63.
947 Quintana, I.M., Gibhardt, J., Turdiev, A., Hammer, E., Commichau, F.M., Lee, V.T., Magni, C.,
948 and Stulke, J. (2019) The KupA and KupB Proteins of Lactococcus lactis IL1403 Are
949 Novel c-di-AMP Receptor Proteins Responsible for Potassium Uptake. *J Bacteriol* **201**.
950 Quintero-Yanes, A., Mayard, A., and Hallez, R. (2022) The two-component system ChvGI
951 maintains cell envelope homeostasis in Caulobacter crescentus. *PLoS Genet* **18**:
952 e1010465.
953 Quintero-Yanes, A., Monson, R.E., and Salmond, G.P.C. (2019) Environmental potassium
954 regulates bacterial flotation, antibiotic production and turgor pressure in Serratia
955 through the TrkH transporter. *Environ Microbiol* **21**: 2499-2510.
956 Rasmussen, T. (2023) The Potassium Efflux System Kef: Bacterial Protection against Toxic
957 Electrophilic Compounds. *Membranes (Basel)* **13**.
958 Rhoads, D.B., Waters, F.B., and Epstein, W. (1976) Cation transport in Escherichia coli. VIII.
959 Potassium transport mutants. *J Gen Physiol* **67**: 325-341.
960 Roe, A.J., McLaggan, D., O'Byrne, C.P., and Booth, I.R. (2000) Rapid inactivation of the
961 Escherichia coli Kdp K+ uptake system by high potassium concentrations. *Mol*
962 *Microbiol* **35**: 1235-1243.
963 Ronneau, S., Petit, K., De Bolle, X., and Hallez, R. (2016) Phosphotransferase-dependent
964 accumulation of (p)ppGpp in response to glutamine deprivation in Caulobacter
965 crescentus. *Nat Commun* **7**: 11423.
966 Roosild, T.P., Castronovo, S., Healy, J., Miller, S., Pliotas, C., Rasmussen, T., Bartlett, W.,
967 Conway, S.J., and Booth, I.R. (2010) Mechanism of ligand-gated potassium efflux in
968 bacterial pathogens. *Proc Natl Acad Sci U S A* **107**: 19784-19789.
969 Rozov, A., Khusainov, I., El Omari, K., Duman, R., Mykhaylyk, V., Yusupov, M., Westhof, E.,
970 Wagner, A., and Yusupova, G. (2019) Importance of potassium ions for ribosome
971 structure and function revealed by long-wavelength X-ray diffraction. *Nat Commun* **10**:
972 2519.

973 Sato, Y., Nanatani, K., Hamamoto, S., Shimizu, M., Takahashi, M., Tabuchi-Kobayashi, M.,
974 Mizutani, A., Schroeder, J.I., Souma, S., and Uozumi, N. (2014) Defining membrane
975 spanning domains and crucial membrane-localized acidic amino acid residues for K(+)
976 transport of a Kup/HAK/KT-type Escherichia coli potassium transporter. *J Biochem* **155**:
977 315-323.
978 Schleyer, M., and Bakker, E.P. (1993) Nucleotide sequence and 3'-end deletion studies indicate
979 that the K(+)-uptake protein kup from Escherichia coli is composed of a hydrophobic
980 core linked to a large and partially essential hydrophilic C terminus. *J Bacteriol* **175**:
981 6925-6931.
982 Schramke, H., Laermann, V., Tegetmeyer, H.E., Brachmann, A., Jung, K., and Altendorf, K.
983 (2017) Revisiting regulation of potassium homeostasis in Escherichia coli: the
984 connection to phosphate limitation. *Microbiologyopen* **6**.
985 Schramke, H., Tostevin, F., Heermann, R., Gerland, U., and Jung, K. (2016) A Dual-Sensing
986 Receptor Confers Robust Cellular Homeostasis. *Cell Rep* **16**: 213-221.
987 Shyp, V., Dubey, B.N., Bohm, R., Hartl, J., Nesper, J., Vorholt, J.A., Hiller, S., Schirmer, T., and
988 Jenal, U. (2021) Reciprocal growth control by competitive binding of nucleotide second
989 messengers to a metabolic switch in Caulobacter crescentus. *Nat Microbiol* **6**: 59-72.
990 Su, J., Gong, H., Lai, J., Main, A., and Lu, S. (2009) The potassium transporter Trk and external
991 potassium modulate Salmonella enterica protein secretion and virulence. *Infect*
992 *Immun* **77**: 667-675.
993 Trchounian, A., and Kobayashi, H. (1999) Kup is the major K+ uptake system in Escherichia coli
994 upon hyper-osmotic stress at a low pH. *FEBS Lett* **447**: 144-148.
995 UniProt, C. (2023) UniProt: the Universal Protein Knowledgebase in 2023. *Nucleic Acids Res*
996 **51**: D523-D531.
997 Untiet, V., Karunakaran, R., Kramer, M., Poole, P., Priefer, U., and Prell, J. (2013) ABC transport
998 is inactivated by the PTS(Ntr) under potassium limitation in Rhizobium leguminosarum
999 3841. *PLoS One* **8**: e64682.
1000 Valente, R.S., and Xavier, K.B. (2016) The Trk Potassium Transporter Is Required for RsmB-
1001 Mediated Activation of Virulence in the Phytopathogen Pectobacterium wasabiae. *J*
1002 *Bacteriol* **198**: 248-255.
1003 Zakharyan, E., and Trchounian, A. (2001) K+ influx by Kup in Escherichia coli is accompanied
1004 by a decrease in H+ efflux. *FEMS Microbiol Lett* **204**: 61-64.
1005 Zimmer, B., Hillmann, A., and Gorke, B. (2008) Requirements for the phosphorylation of the
1006 Escherichia coli EIIANtr protein in vivo. *FEMS Microbiol Lett* **286**: 96-102.

1007

1008

1009

1010

1011

1012 **Figures**

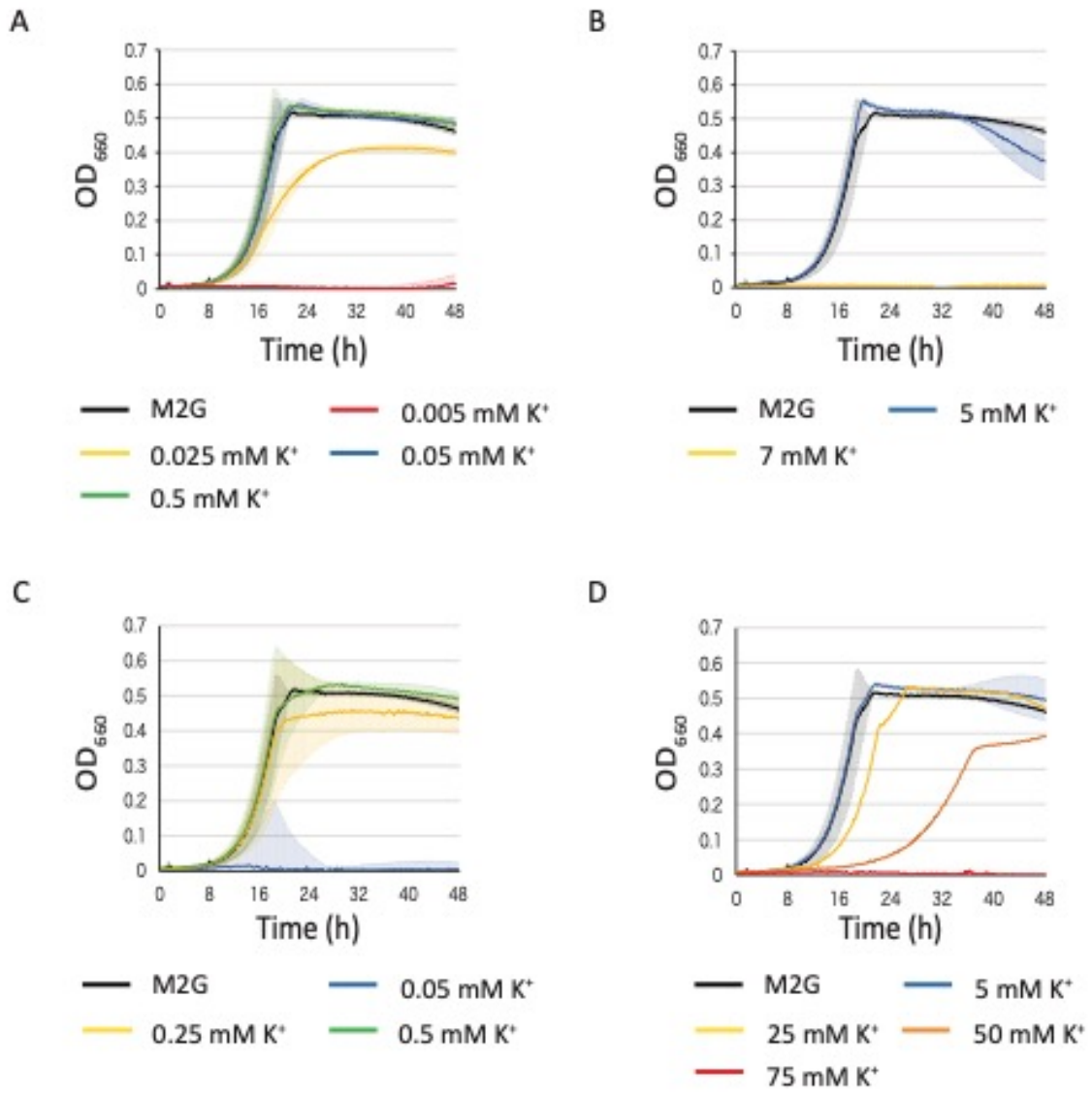

1013

1014 **Figure 1. Impact of K^+ on *C. crescentus* growth.** Growth of WT in M2G-K
1015 supplemented with different K^+ concentrations using K_2HPO_4 + KH_2PO_4 (A-B) and KCl
1016 (C-D) as K^+ source. Data represent average, n=3, and error bars= ±SD. Other
1017 concentrations tested are presented in Fig. S1.

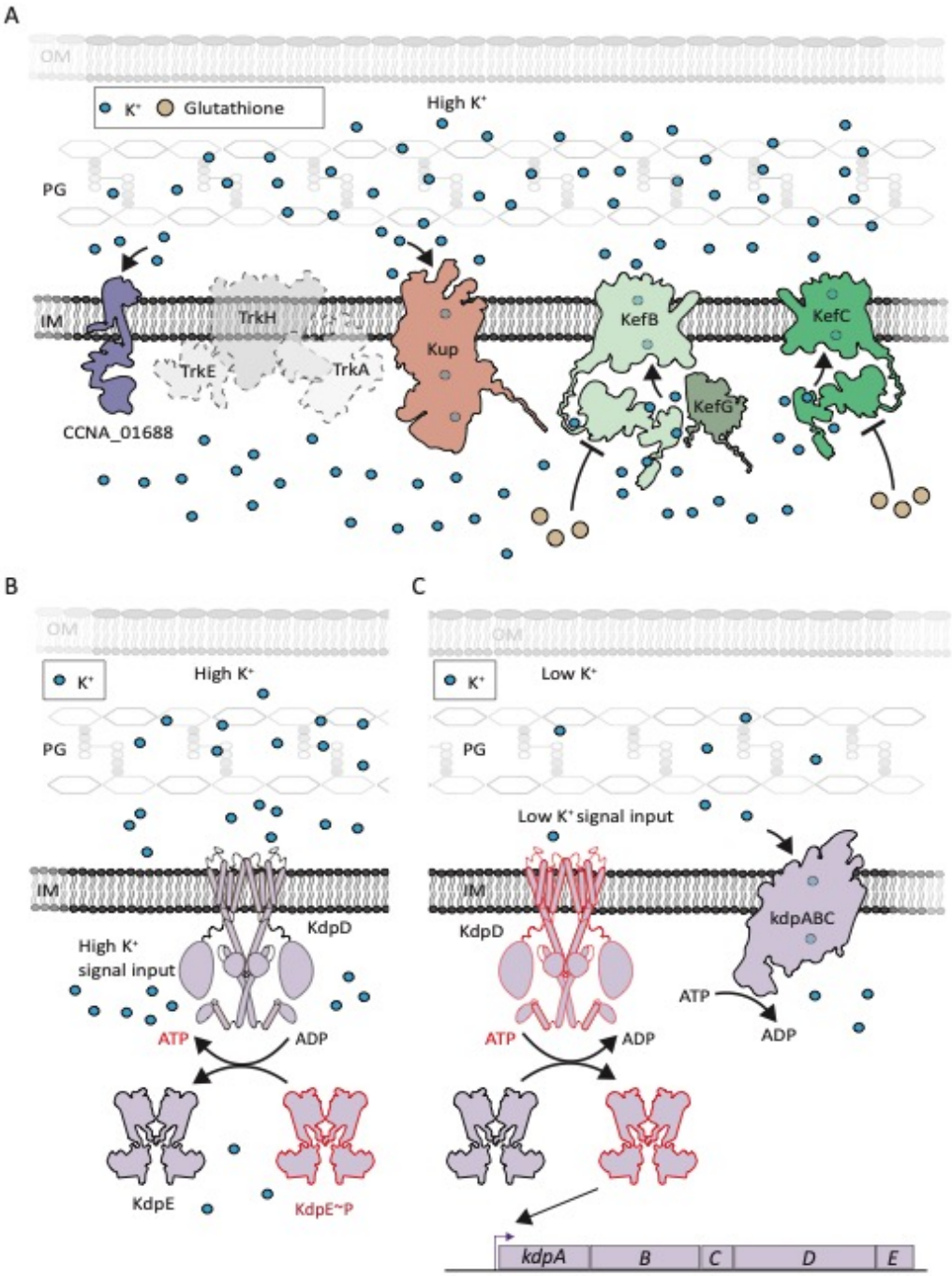

1018

1019 **Figure 2. K^+ transport and response systems in Gram-negative bacteria**.
1020 Schematic diagram of K^+-related proteins predicted to work at high (A-B) or low (C) K^+
1021 concentrations. Coloured proteins correspond to the ones encoded in *C. crescentus*
1022 genome: CCNA_01688, Kup (CCNA_00130), KefB (CCNA_00204), KefG
1023 (CCNA_00205), KefC (CCNA_03611), KdpDE (CCNA_01666-CCNA_01667)

1024 KdpFABC (CCNA_01662-CCNA_01665). The genes were identified using Biocyc
1025 collection of microbial genomes (Karp *et al.*, 2019) and structures of the proteins
1026 obtained using predictions with alphafold from Uniprot (UniProt, 2023). Outer
1027 Membrane (OM), peptidoglycan (PG), inner membrane (IM).

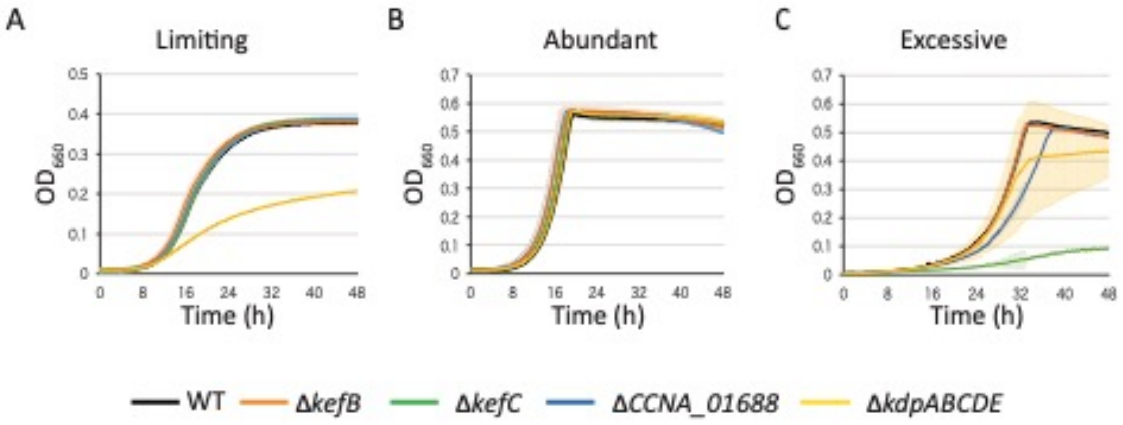

1028

1029 **Figure 3. Deletion of K^+-related genes impact *C. crescentus* growth.** Growth of
1030 WT, Δ*kefB*, Δ*kefC*, ΔCCNA_01688 and Δ*kdpABCDE* mutants in minimal media M2G-
1031 K supplemented with (A) limiting (0.025 mM), (B) abundant (0.5 mM) and (C) excessive
1032 (50 mM) K^+ concentrations. Data represent average, n=3, and error bars= ±SD.

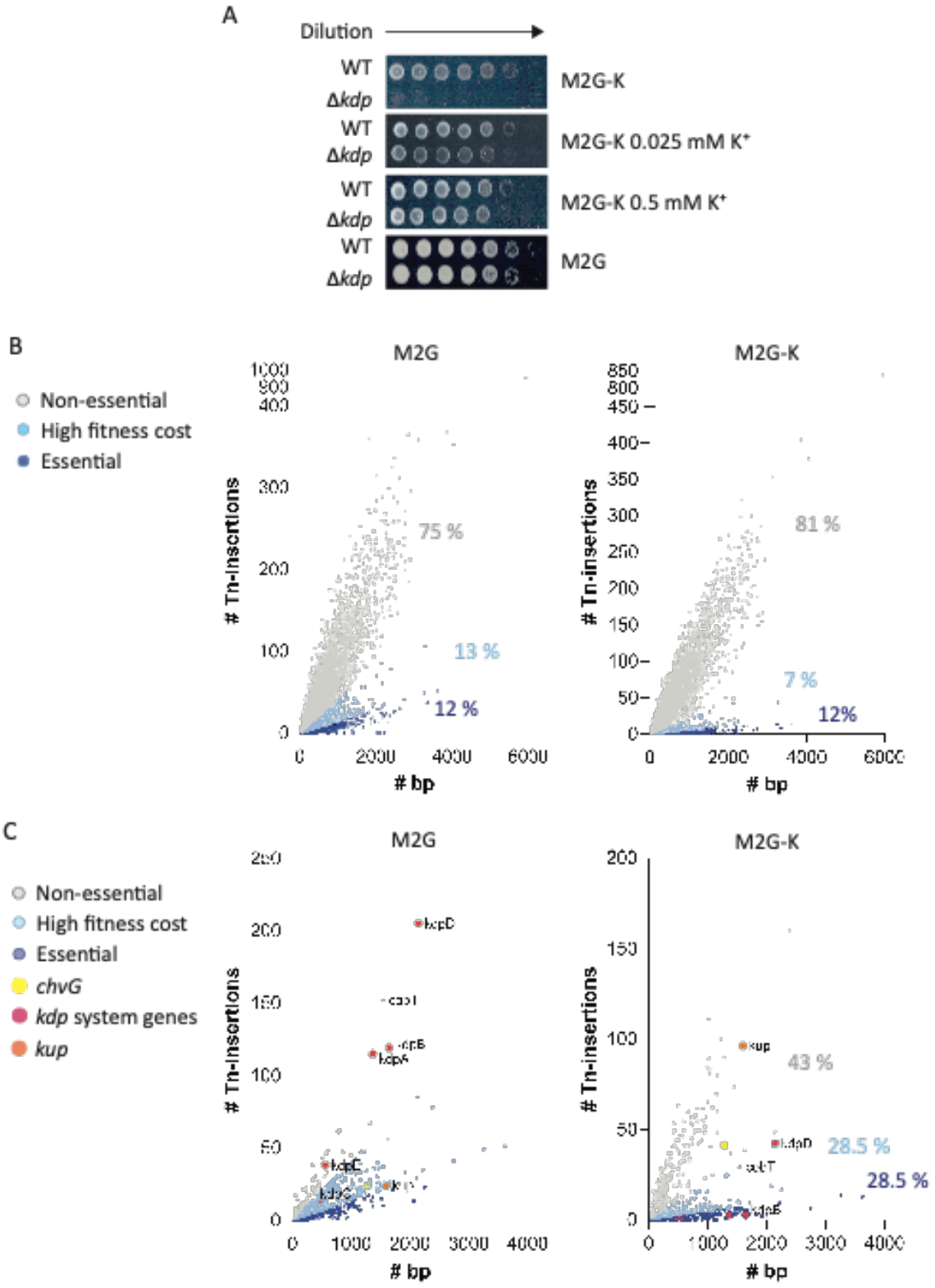

1033

1034 **Figure 4. Tn-seq and RNA-seq profile of *C. crescentus* cells in limiting K⁺**

1035 **conditions.** (A) Growth of WT and Δ*kdp* cells in M2G-K plates without or

1036 supplemented with K^+. (B) Number of Transposon-insertions (#Tn-insertions) against
1037 the length (#bp) of 4186 genes in M2G and M2G-K media. Non-essential genes are
1038 highlighted in grey, high-fitness cost genes in light blue, and essential in dark blue. (C)
1039 Representation of genes that changed in their fitness-cost categories according to
1040 analysis done in M2G and M2G-K (B). (B-C) The percentage of genes in each category
1041 is indicated following the colour code.

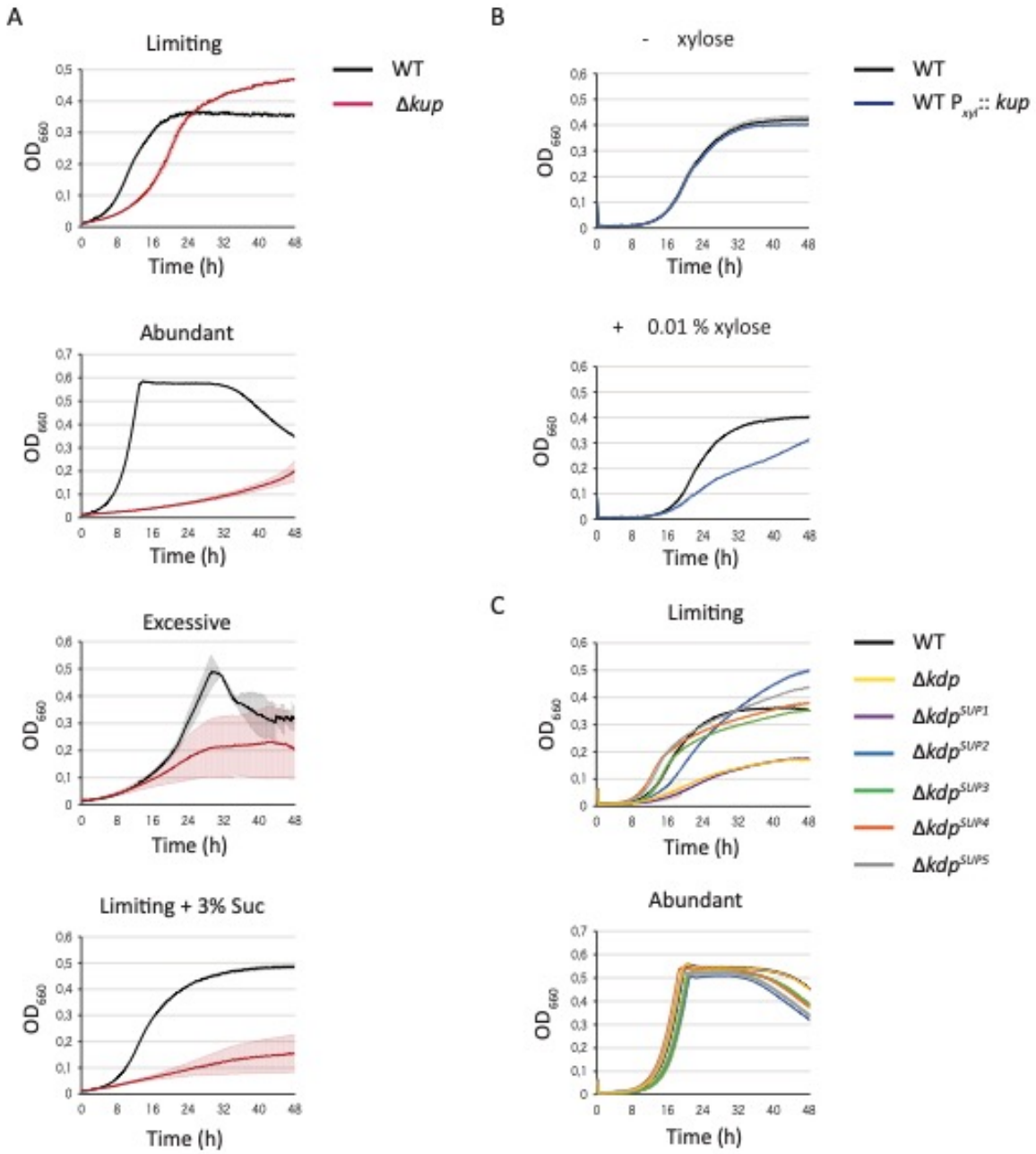

1042

1043 **Figure 5. Impact of deletion and overexpression of the *kup* gene.** (A) Growth of
1044 WT and Δ*kup* mutant in minimal media M2G-K supplemented with limiting (0.025 mM),
1045 abundant (0.5 mM), excessive (50 mM) K^+ concentrations or limiting (0.025 mM) K^+
1046 concentrations and 3% sucrose. (B) Growth of WT expressing *kup* under xylose
1047 induction. (C) Growth of WT, Δ*kdp* and Δ*kdp* suppressors (Δ*kdp*^{SUP}) in minimal media
1048 M2G-K supplemented with limiting (0.025 mM) or abundant (0.5 mM). Data represent
1049 average, n=3, and error bars= ±SD.

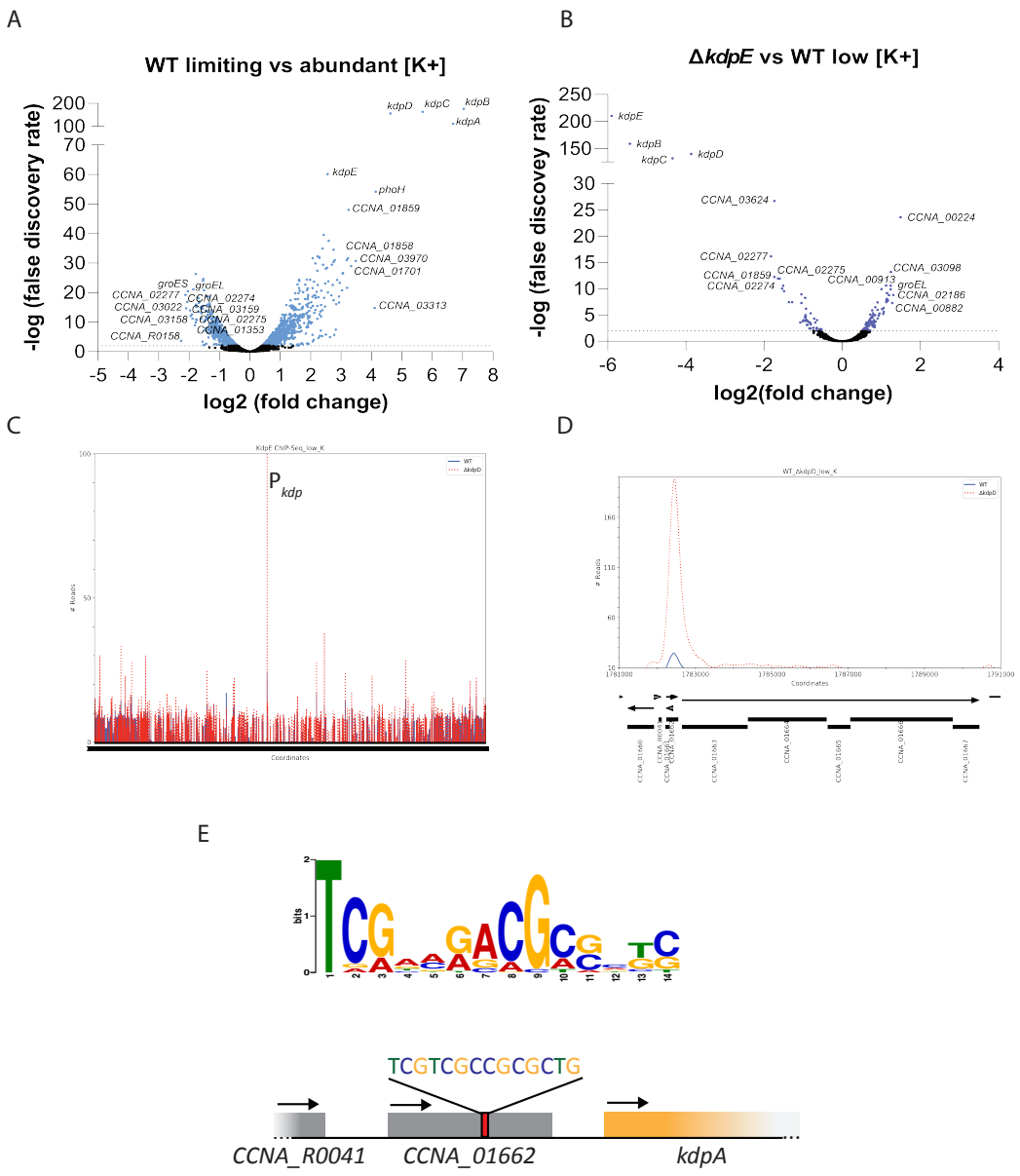

1050

1051 **Figure 6. K^+ and KdpE-dependent regulon.** (A-B) Volcano plots representing the
1052 relation between the log_2 fold change (FC) and -log False Discovery Rate (FDR) on
1053 gene expression between (A) WT in limiting *vs* abundant K^+ condition, and (B) Δ*kdpE*
1054 vs WT in limiting K^+ condition. Genes identified are presented as dots. Significant
1055 down- and up-regulated genes are presented as blue (A) and purple (B) dots, while
1056 genes with no significant alterations are presented as black dots. Top 10 down and
1057 upregulated genes are highlighted for each analysis. (C) Genome-wide occupancy of
1058 KdpE on the chromosome of *C. crescentus* determined by ChIP-seq on Δ*kdpE*
1059 P_{xylX}::*kdpE* Δ*xylX* and Δ*kdpDE* P_{xylX}::*kdpE* Δ*xylX*. The x-axis represents the coordinates
1060 on the genome (Mb), the y-axis shows the normalized ChIP-Seq read abundance in
1061 reads. The promoter region of *kdp* is highlighted. (D) Occupancy of KdpE on the *kdp*
1062 promoter Δ*kdpE* P_{xylX}::*kdpE* Δ*xylX* and Δ*kdpDE* P_{xylX}::*kdpE* Δ*xylX*. (E) WebLogo of
1063 predicted KdpE consensus sequence obtained with MEME and identification (with a *p-*
1064 *value* 7.71 x 10^{-5}) of the DNA binding sequence upstream of *kdpA.* Arrows indicate
1065 gene orientation for expression.

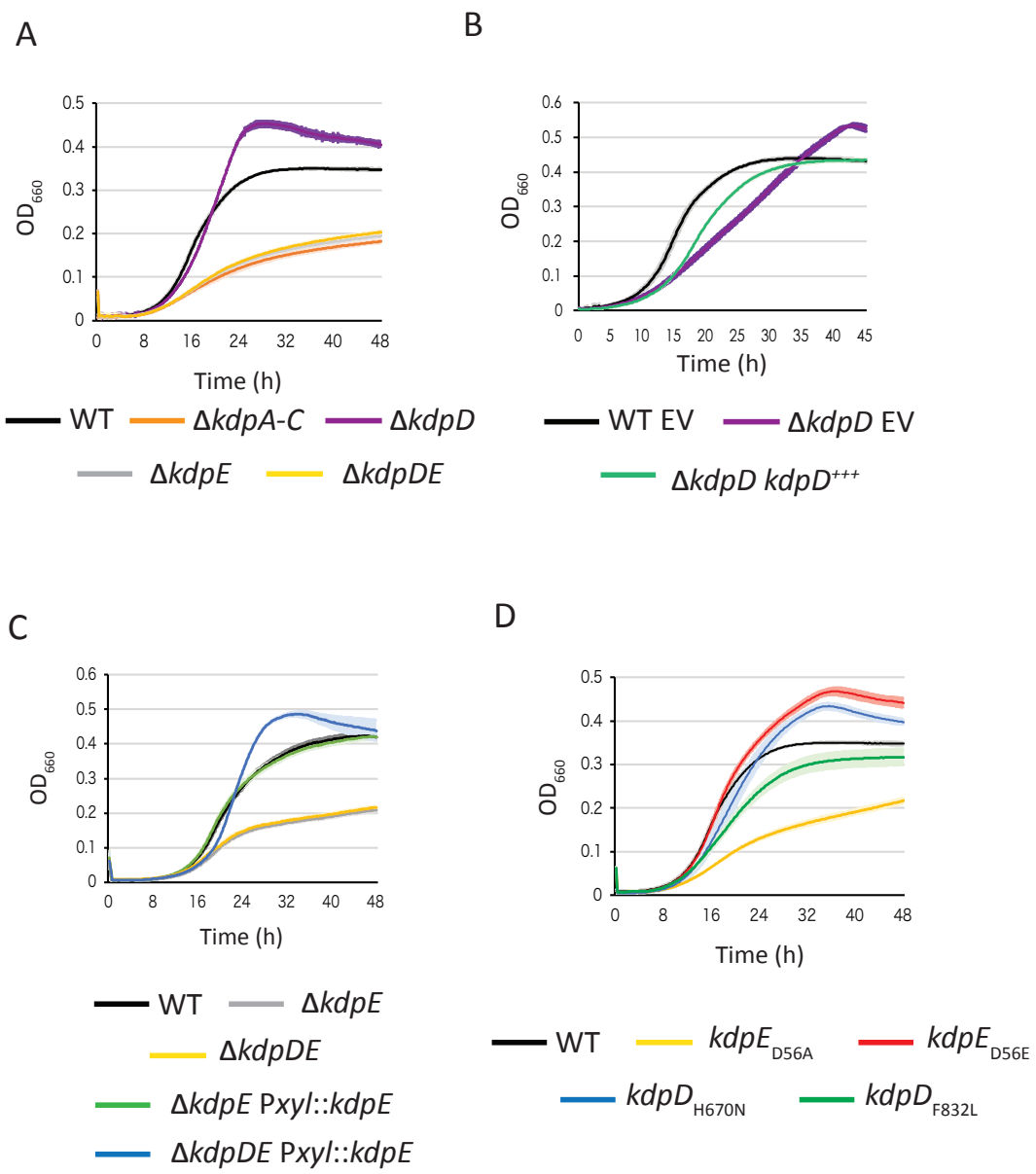

1066

1067 **Figure 7. KdpD downregulates KdpE to control growth in low K⁺.** (A) Growth of
1068 WT, Δ*kdpABC,* Δ*kdpD*, Δ*kdpE* and Δ*kdpDE*. (B) Growth of WT and Δ*kdpD* carrying
1069 either pMR10 empty vectors (EV) or pMR10 P_{kdp}*::kdpD*. (C) Growth of WT, Δ*kdpE*,
1070 Δ*kdpDE* expressing *kdpE* from the *xylX* locus (P_{xylX}*::kdpE*). (D) Growth of *kdpD* and
1071 *kdpE* catalytic point mutants. Growth was done in minimal media M2G-K
1072 supplemented with limiting (0.025 mM) K^+ concentrations (A-D), media was
1073 additionally supplemented tetracycline for plasmid selection (B) or with 0.01 % xylose

1074 for the induction of *kdpE* expression (C). Data represent average, n=3, and error bars=

1075 ±SD.

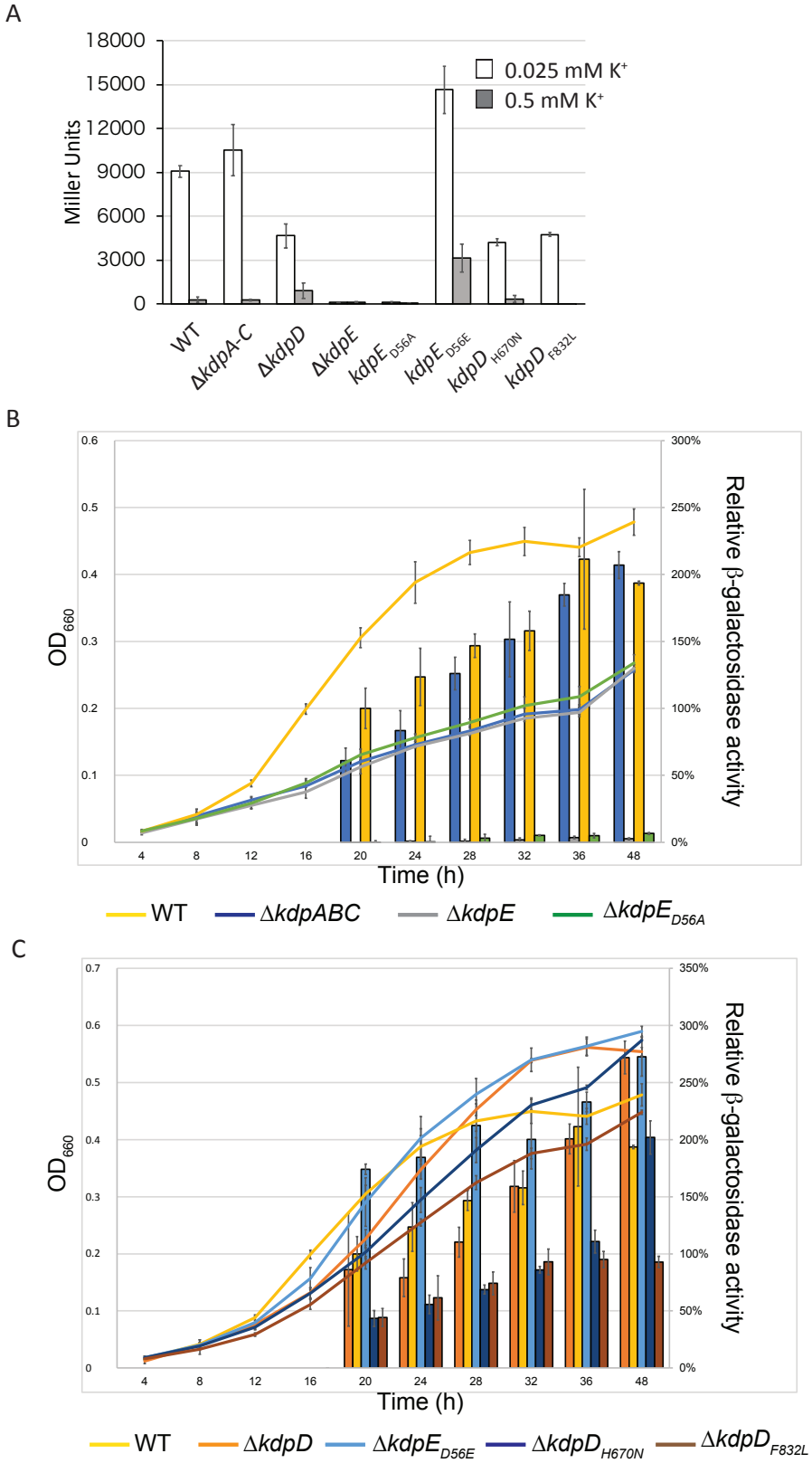

1076

1077 **Figure 8. Regulation of *kdp* expression** (A) β-Galactosidase activities of WT and *kdp*
1078 mutants carrying a transcriptional P_{kdp}::*lacZ* fusion grown in M2G-K supplemented with
1079 limiting (0.025 mM) or abundant (0.5 mM). β-Galactosidase activities of WT and *kdp*
1080 mutants carrying a transcriptional P_{kdp}::*lacZ* fusion along the growth in M2G-K
1081 supplemented with limiting (0.025 mM). Statistical analyses were carried out via single
1082 factor ANOVA. Data represent average, n=3, and error bars= ±SD.

1083

1084

1085

1086

1087

1088

1089

1090

1091

1092

1093